

**Experimental Study of Engine Oil Film Thickness Dependence on Liner Location,  
Oil Properties and Operating Conditions**

by

Goro Tamai

B. S., Mechanical Engineering; Massachusetts Institute of Technology, 1993

Submitted to the Department Mechanical Engineering in Partial Fulfillment of the  
Requirements for the Degrees of

MASTER OF SCIENCE IN MECHANICAL ENGINEERING

at the

Massachusetts Institute of Technology; August 1995

© 1995 Goro Tamai. All rights reserved.

The author hereby grants to MIT permission to reproduce and to distribute publicly paper  
and electronic copies of this document in whole or in part.

Signature of Author \_\_\_\_\_  
Department of Mechanical Engineering, August 1995

Certified by \_\_\_\_\_  
Dr. Victor W. Wong  
Lecturer, Department of Mechanical Engineering  
Thesis Advisor

Accepted by \_\_\_\_\_  
A. A. Sonin, Chairman  
Departmental Committee on Graduate Studies  
Department of Mechanical Engineering

MASSACHUSETTS INSTITUTE  
OF TECHNOLOGY

SEP 21 1995

ARCHIVES

LIBRARIES

**(This page intentionally left blank)**

# **Experimental Study of Engine Oil Film Thickness Dependence on Liner Location, Oil Properties and Operating Conditions**

by  
Goro Tamai

Submitted to the Department of Mechanical Engineering on August 11, 1995 in Partial Fulfillment of the Requirements for the Degrees of Master of Science in Mechanical Engineering.

## **ABSTRACT**

The oil film thickness was measured in a single-cylinder spark-ignition engine via the Laser Induced Fluorescence (LIF) technique. The laser accessed the cylinder liner through a quartz window at six locations. An array of four windows were located circumferentially at midstroke, and one window was located on the thrust side near each endstroke. Of the six windows, three midstroke windows and the bottom center window were operational. The objective of the experiments was to investigate how the oil film thickness varies with cylinder liner location, oil properties, and engine running conditions. In addition, the relative film thicknesses under and around each piston ring was observed. Finally, the resolution of the LIF system was increased to gain a better picture of the oil control rails whose oil behavior has been difficult to assess in the past due to its narrow width.

In order to ensure accurate film thickness results, great attention was paid to the micro-geometry of the engine components such as: LIF window flushness, cylinder liner surface roughness, cylinder bore distortion, piston surface features, and ring race profiles. The calibration of the LIF signal was performed referencing the piston skirt machining marks and the oil control rail face contours. The calibration constants obtained from the two methods were very consistent.

The experimental results show that the bore distortion effects are significant and noticeable from the circumferential film thickness data. A radial bore distortion of 15 microns, measured in a cold engine block, resulted in circumferential film thickness differences of a factor of two to three. The top ring minimum film thickness at midstroke for the baseline running condition (fired at 2500 rpm, 100 deg. C, bmep=631 kPa) with SAE 50 oil ranged from 0.7 microns to 1.8 microns. The film thickness at midstroke was typically about a factor of 1.5 greater than that at bottom center on the thrust side.

The experimental film thickness trends for oil viscosity and engine speed were both reasonable. The film thickness for the SAE 50 oil was about 65% greater than that for the SAE 10W oil. The film thickness for the baseline engine speed of 2500 rpm was about 20 % greater than that for a speed of 1800 rpm.

Other interesting observations include: the film thickness under the lower oil control rail was thicker than that of the upper oil control rail for both the up and down strokes, the shear-thinning effect of the multi-grade 10w50 oil, the inertia effect on oil masses on the lands, the effect of piston skirt size on film thickness trends, and the presence or absence of oil on the crown and second lands depending on operating condition.

Thesis Supervisor: Victor W. Wong  
Title: Lecturer, Department of Mechanical Engineering

**(This page intentionally left blank)**

## ACKNOWLEDGMENTS

I would first like to thank the faculty at MIT Sloan Automotive Lab that made my stay here as a graduate student pleasant and exciting. In particular, my advisor Dr. Victor Wong, who has supported me through my undergraduate thesis, all the way through my Master's. His guidance and support was irreplaceable. Also on my thank you list are Dr. David Hoult, Prof. John Heywood and Prof. Wai Cheng.

The second bunch of people I'd like to thank are my fellow students that I worked along side with at the Sloan Lab. First my officemates: Tian Tian, the theory man, who I could never have gotten through this thesis project and some of my classes without, and taught me five words in Chinese; and Bouke Noordzij the Harley biker who can setup an engine experiment in record time and neatness. Also, Luis Palacios, the best UROP any grad student could ever ask for - he did everything from helping run the experiments to setting up computer hardware to telling great frat stories. I'd also like to thank the rest of the Sloan folks who helped make my stay here more enjoyable: Mike Norris, Gatis Bazbauers, Denis Artzner, Vincent Frottier, Jon Fox, Captain Mark Lusted, Mike Bush, Eric Deutsch, Leon Bronchstein, Jim Ryan, Paul Llamas, Younggy Shin, Doug Schofield, Eric Ford, Wolf Bauer, Janice Dearlove, Peter Hinze, Richard Versteegh, Joan Kenney, Brian Corkum, Viktor Dubrowski, Don Fitzgerald, and Nancy Cook. And thank you to my parents and brother for all their support and understanding.

Since I promised my girlfriend Kathy her very own paragraph, here it is. I'd like to thank her for all her love, support and understanding through all the highs and lows throughout my whole (at least almost) MIT career. I don't think I could have ever made it through without her.

Finally, since this marks the end of my six year MIT career, I'd like to thank some very special people who I met at MIT that have made a world of difference to me: Thomas Massie, Dr. Erik Vaaler, Prof. Gill Pratt, James Worden, Peter Rexer, Olaf Bleck, Jackie Martling, and the entire SEVT, with particular mention to Maraka, Milf, How, Unchi, Iv'no and Grockamouli from the 1993 -1995 seasons.

This work has been supported by the Consortium of Lubrication in Internal Combustion Engines, whose members over the course of this work include: Shell Oil Company, Pennzoil Products, Dana Corporation, Peugeot, Renault. The U.S. Coast Guard, D.O.T. Maritime Administration, and Cummins Engine Company also made direct or in-kind contributions. I would like to thank in particular Dr. Phil Burnett at Shell, and Dr. Selda Gonsel and her research staff at Pennzoil, and David Fiedler at Dana for their technical support. I would also like to thank the engineering staff at Kohler for their technical assistance.

Goro Tamai,  
August, 1995

**(This page intentionally left blank)**

## TABLE OF CONTENTS

ABSTRACT	3
ACKNOWLEDGMENTS	5
TABLE OF CONTENTS	7
LIST OF FIGURES	9
LIST OF TABLES	12
LIST OF ABBREVIATIONS	13
Chapter 1 MOTIVATION	14
1.1 Introduction	14
1.2 Previous Work	15
1.3 Project Objectives	15
Chapter 2 EXPERIMENTAL APPARATUS	17
2.1 Laser Induced Fluorescence (LIF) System	17
2.2 The Engine: Kohler CH-14 Single-Cylinder Spark Ignition Engine with LIF Windows	22
2.2.1 LIF Window Locations	26
2.2.2 Cylinder Liner Thermocouples	29
2.2.3 Cylinder Pressure Transducer	30
2.3 Data Acquisition System	31
Chapter 3 TEST OILS	33
3.1 Oil Viscosity vs. Temperature	33
3.2 Mono-Grade vs. Multi-Grade Oils	35
Chapter 4 TEST MATRIX	38
Chapter 5 MICRO-MEASUREMENT OF ENGINE COMPONENTS	40
5.1 Engine Block Micro-Geometry	40
5.2 Piston and Piston Ring Micro-Geometry	43
Chapter 6 DATA PROCESSING	47
6.1 Raw LIF Data	47
6.2 Zero Offset	48
6.3 Engine Kinematics	48
6.4 LIF Oil Film Calibration	51

6.4.1 Piston Upper Skirt Tool Marks Calibration Method	51
6.4.2 Oil Control Rail Calibration Method	53
6.4.3 LIF Calibration for Top Center Window	56
6.4.4 LIF Calibration vs. Liner Temperature and Oil Grade	58
6.5 Accuracy Tolerance of LIF Oil Film Thickness	59
Chapter 7 THEORY	60
7.1 Piston Ring Lubrication Theory	60
7.1.1 Oil Film Thickness Calculation	61
7.1.2 Wedge Effect	63
7.1.3 Corner Effect	64
7.1.4 Squeeze Effect	64
Chapter 8 EXPERIMENTAL RESULTS AND ANALYSIS	66
8.1 Relative Film Thicknesses Among the Free Liner and the Top Two Rings	67
8.2 Liner Location Trend	72
8.3 Oil Viscosity and Temperature Trends	75
8.4 Engine Speed Trend	77
8.5 Observations of Oil Masses on Piston Lands and Skirt	78
Chapter 9 CONCLUSIONS	81
Chapter 10 RECOMMENDATIONS	83
10.1 Future Experimental Work	83
10.2 LIF System Recommendation	83
REFERENCES	85
Appendix A COMMON REFERENCE NUMBERS	87
Appendix B SAMPLE TEST RECORDING	88
Appendix C LIF CALIBRATION COEFFICIENTS	92
Appendix D ADDITIONAL LIF FILM THICKNESS PLOTS	93

## LIST OF FIGURES

Figure 2.1 Schematic of Laser Induced Fluorescence System.	17
Figure 2.2 Average PMT noise vs. PMT voltage.	19
Figure 2.3 LIF probe/window locations and window number convention of Kohler engine. (Deutsch Thesis [3])	25
Figure 2.4 Crank angle positions for each ring at each window location in Kohler engine	26
Figure 2.5 Instantaneous piston speed vs. crank angle for Kohler engine at 2500 rpm.	27
Figure 2.6 Typical LIF midstroke trace.	28
Figure 2.7 LIF trace from the bottom center window (win. #6). Notice that the spatial sampling rate when window #6 sees the top of the piston (where piston velocity is low) is higher than that when the window sees the piston skirt.	29
Figure 3.1 Viscosity vs. Temperature for multi and mono-grade oils. Notice non-linearity of viscosity trend.	34
Figure 3.2 Viscosity vs. Temperature for multi and mono-grade oils on semilog scale.	34
Figure 3.3 Viscosity vs. shear rate relationship from the Cross Equation.	36
Figure 4.1 Shell test matrix for multi-LIF probe Kohler engine.	39
Figure 5.1 Bore distortion plot at midstroke. Scale = 2 microns per division, maximum radial difference = 20 microns, max radial difference between windows = 16 microns (window #1 vs. window #2).	41
Figure 5.2 Talysurf trace of window-to-liner check at window #4. Maximum window protrusion into liner is about one micron.	42
Figure 5.3 Talysurf of Kohler top ring.	44
Figure 5.4 Talysurf of Kohler 2nd ring.	44
Figure 5.5 Talysurf of Kohler upper skirt machining marks.	45
Figure 5.6 Talysurf of Kohler oil control rails.	45
Figure 6.1 Full cycle of LIF data starting from the beginning of the intake stroke.	47

Figure 6.2 Schematic of Kohler piston assembly.	49
Figure 6.3 Calibration of LIF signal by matching a segment of an LIF trace to upper-skirt machining marks.	52
Figure 6.4 Upper OC rail fit into LIF trace for signal calibration.	54
Figure 6.5 LIF calibration graph showing OC rail fit along with skirt machining mark match.	55
Figure 6.6 Laser beam impinging on OC rail at different wedge locations.	55
Figure 6.7 Illustration of how an over-flooded lower OC rail results in an LIF trace too narrow for the OC rail Talysurf profile.	57
Figure 6.8 Good lower OC rail fit.	57
Figure 7.1: Schematic of ring and liner and its coordinate system definition. Plot below shows pressure distribution under ring which produces lift.	60
Figure 8.1 Example of the improved resolution OC rail trace.	63
Figure 8.2 MOFT vs. liner location. Shows trends of: windows (circumferential, axial), rings, speed (mid vs. BDC) for SAE 10w oil.	67
Figure 8.3: Schematic of the hierarchy of the MOFT's under the piston rings.	68
Figure 8.4 MOFT vs. liner location. Shows trends of: windows (circumferential, axial), rings, speed (mid vs. BDC) for 10w50 oil.	71
Figure 8.5 MOFT vs. liner location. Shows trends of: windows (circumferential, axial), rings, speed (mid vs. BDC) for SAE 50 oil.	72
Figure 8.6 Top ring MOFT vs. oil grade vs. liner location. Shows trend of: windows, skirt, and oil viscosity. Clearly illustrates viscosity trend for each window.	73
Figure 8.7 Free-liner film thickness vs. liner temperature vs. oil grade. Shows trend of: liner temperature, oil viscosity, shear-thinning effect. Notice that low temperature SAE 50 oil's film thickness is relatively small. The trends generally hold for the top two rings also.	74
Figure 8.8 Upper OC rail MOFT vs. liner temperature vs. oil grade. Shows trends of: liner temperature, oil viscosity, shear-thinning effect. For OC rails, the low temperature SAE 50 oil's film thickness is not relatively small, as in Figure 8.6.	74
Figure 8.9 Free-liner film thickness vs. engine speed vs. oil grade. Shows trend of: engine rpm, oil viscosity, and shear-thinning.	75
Figure 8.10(a) Third land oil volume skewed due to oil mass inertia.	79
Figure 8.10(b) Third land oil volume skewed due to oil mass inertia.	79

Figure 8.11(a) Wet 2nd land for baseline running condition at window #1. \_\_\_\_\_ 80

Figure 8.11(b) Dry 2nd land for baseline running condition at window #2. \_\_\_\_\_ 80

Figure D.1 MOFT vs. liner location for the compression stroke. Shows trends of: windows (circumferential, axial), rings, speed (mid vs. BDC) for SAE 10w oil. Data has been averaged over ten cycles. \_\_\_\_\_ 93

Figure D.2 MOFT vs. liner location for the expansion stroke. Shows trends of: windows (circumferential, axial), rings, speed (mid vs. BDC) for SAE 10w oil. Data has been averaged over ten cycles. \_\_\_\_\_ 93

Figure D.3 MOFT vs. liner location for the exhaust stroke. Shows trends of: windows (circumferential, axial), rings, speed (mid vs. BDC) for SAE 10w oil. Data has been averaged over ten cycles. \_\_\_\_\_ 94

Figure D.4 Free-liner film thickness vs. oil grade vs. liner location. Shows trend of: windows, skirt, and oil viscosity. Clearly illustrates viscosity trend for each window. Data has been averaged over ten cycles. Recall that the free-liner is not seen from window #6 (BDC). \_\_\_\_\_ 94

Figure D.5 Lower OC rail MOFT vs. oil grade vs. liner location. Shows trend of: windows, skirt, and oil viscosity. Clearly illustrates viscosity trend for each window. Data has been averaged over ten cycles. \_\_\_\_\_ 95

## LIST OF TABLES

Table 2.1 Components of the MIT LIF system.	22
Table 2.2 Kohler engine specifications.	22
Table 2.3 Engine component temperature data by Furuhamma et al, and French et al showing that top center cylinder temperature is very close to that of the upper piston skirt.	30
Table 6.1 PMT voltage for various liner temperatures.	59
Table B.1 Sample test recording sheet.	88
Table C.1 LIF calibration coefficients for fired data sets.	90

## LIST OF ABBREVIATIONS

LIF \_\_\_\_\_ Laser Induced Fluorescence

OC Rails \_\_\_\_\_ Oil Control Rails

MOFT \_\_\_\_\_ Minimum Oil Film Thickness

TDC \_\_\_\_\_ Top Dead Center

BDC \_\_\_\_\_ Bottom Dead Center

## CHAPTER 1: MOTIVATION

### 1.1 INTRODUCTION

One of the most commonly asked questions is why a particular research project is important; in this case, why lubrication study is important. Engine lubrication research is important for a number of reasons. From the societal view point, in this increasingly energy-stringent society, every bit of energy wasted is frowned upon. Therefore, thoroughly understanding the role of the lubricant film inside an engine is vital to minimizing engine friction, and boosting engine fuel efficiency. From the technical view point, lubrication research is a complicated puzzle with many facets. The lubrication engineer must juggle engine friction, oil consumption, component wear, oil recyclability, cost, etc. The lubrication engineer's job has become increasingly difficult over the past ten years. Engines are getting more powerful, run at higher engine speeds, consume less oil, have less oil in the sump, have longer drain intervals, and run hotter as power density increases. In fact, according to a recent study by Shell, the oil stress factor has increased three fold in the last decade [1].

The focus of this study is the oil layer between the piston rings and the engine cylinder liner. This is perhaps the most vital area of engine lubrication study, for ring pack friction makes up close to 50% of overall engine rubbing friction, and oil lost via transport through the ring pack represents 80 - 90% of the total oil consumed by the engine in some cases [2].

The MIT Laser Induced Fluorescence (LIF) system for measuring oil film thickness in an internal combustion engine has been under development for almost ten years. Over the years, the optical mirrors have been replaced by fiber optic cables, and the resolution of the LIF system to read fine oil film details has improved dramatically [4].

The general overview of the LIF system is as follows: A laser is beamed into the engine cylinder through a quartz window mounted flush in the cylinder liner. The laser impinges on the oil layer between the liner and the piston ring. The oil, doped with a fluorescent dye, then emits a fluorescent light at a different wavelength. The intensity of this fluorescent light is proportional

to the volume of oil from which the light was emitted. The fluorescence intensity is converted to a voltage signal by a photomultiplier tube, and is recorded by the data acquisition system. Some known geometric feature of an engine component such as the piston skirt tool mark is used as a reference to calibrate the LIF voltage signal to an oil film thickness.

## **1.2 PREVIOUS WORK**

This study is a continuation of the work done by another MIT graduate student, Eric Deutsch. The Deutsch engine had a single LIF window located at midstroke on the thrust side. An extensive test matrix of numerous engine running conditions and 15 oils was carried out. However, the results were inconclusive; the film thickness trends were scattered for the lubricant surface tensions and viscosities [3]. Part of the problem may have been circumferential film thickness variations around the cylinder liner, or window-to-liner flushness.

As Deutsch was finishing up his work, the next generation LIF engine configuration was being designed. The new engine block, with six LIF windows, was inherited by the author for this particular study. Six LIF windows were installed in the liner: a circumferential array of four windows at midstroke, and one window at each endstroke on the thrust side. The goal was to investigate the circumferential variation of the oil film thickness at midstroke, and the oil behavior near the endstrokes. Particular attention was paid to window-to-liner flushness, and a variety of oils with more widespread viscosity parameters were tested.

## **1.3 PROJECT OBJECTIVES**

The objectives of this project are:

- 1) Observe how oil film thickness varies with cylinder liner location.
  - a) Measure circumferential variation in oil film thickness to evaluate effect of bore distortion and ring conformability on oil film thickness. Observing the circumferential distribution of oil is also very useful in developing oil consumption models such as the “Puddle Theory” [4].

b) Measure oil film thickness at endstrokes to study trade-offs between endstroke wear and midstroke friction. For multi-grade oils, this directly ties in with the shear-thinning effect of the lubricant. Since multi-grade oils are non-Newtonian, the viscosity changes with shear rate as the piston travels through the engine stroke.

c) Observe effect of the non-axisymmetry of the piston skirt on ring pack oil behavior. (Piston skirt dimensions are different at three of the circumferential piston locations.)

2) Observe how oil film thickness varies with oil properties.

a) Verify film thickness vs. oil viscosity trends.

b) Observe whether the lubricant shear-thinning effect is noticeable.

3) Observe how oil film thickness varies with engine operating conditions such as engine speed and cylinder liner temperature. Liner temperature is of great concern since an oil temperature change from 50 to 100 deg. C can result in a viscosity decrease of 700 percent.

4) Observe the relative oil film thicknesses under each ring in the piston ring pack. Particular attention will be paid to the oil behavior under and around the oil control (OC) rails to gain a better physical understanding of the role of the OC rails on ring pack lubrication.

5) Utilize LIF data as insight to develop better piston and ring pack lubrication models. These models can be used as development tools by engine component manufacturers in the future.

6) Observe how characteristics of oil accumulation on piston lands and on the skirt vary with (1) through (3) above.

## CHAPTER 2: EXPERIMENTAL APPARATUS

### 2.1 LASER INDUCED FLUORESCENCE (LIF) SYSTEM

The purpose of the MIT LIF system is to measure the oil film thickness inside the engine cylinder while the engine is running. A schematic of the LIF system is shown in Figure 2.1. The laser used is a 14 mW Liconix Helium-Cadmium laser with a wavelength of 442 nm. The beam first passes through a 442 nm optical filter to attenuate extraneous light frequencies. The beam is then focused into a fiber optic cable by an “eccentric coupler.” The cable carries the laser light into a focusing probe which is mounted into the engine block. The laser power output to the engine from the fiber optic cable should be about 3 to 4 mW, depending on the condition of the fiber optic cable. Great care should be paid when adjusting the eccentric coupler to ensure proper laser power transmission.

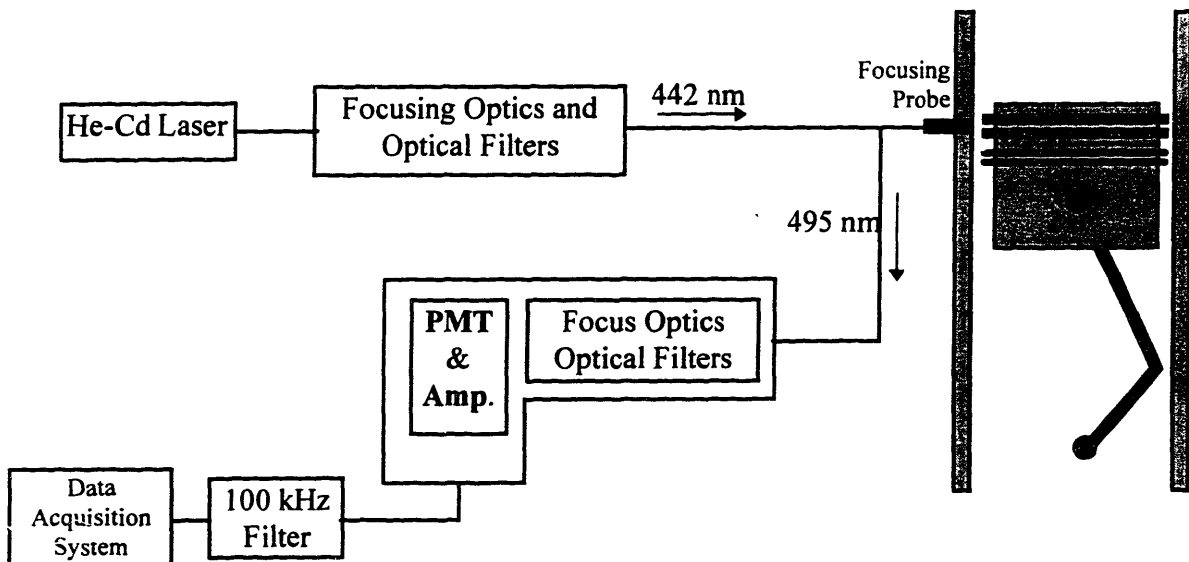


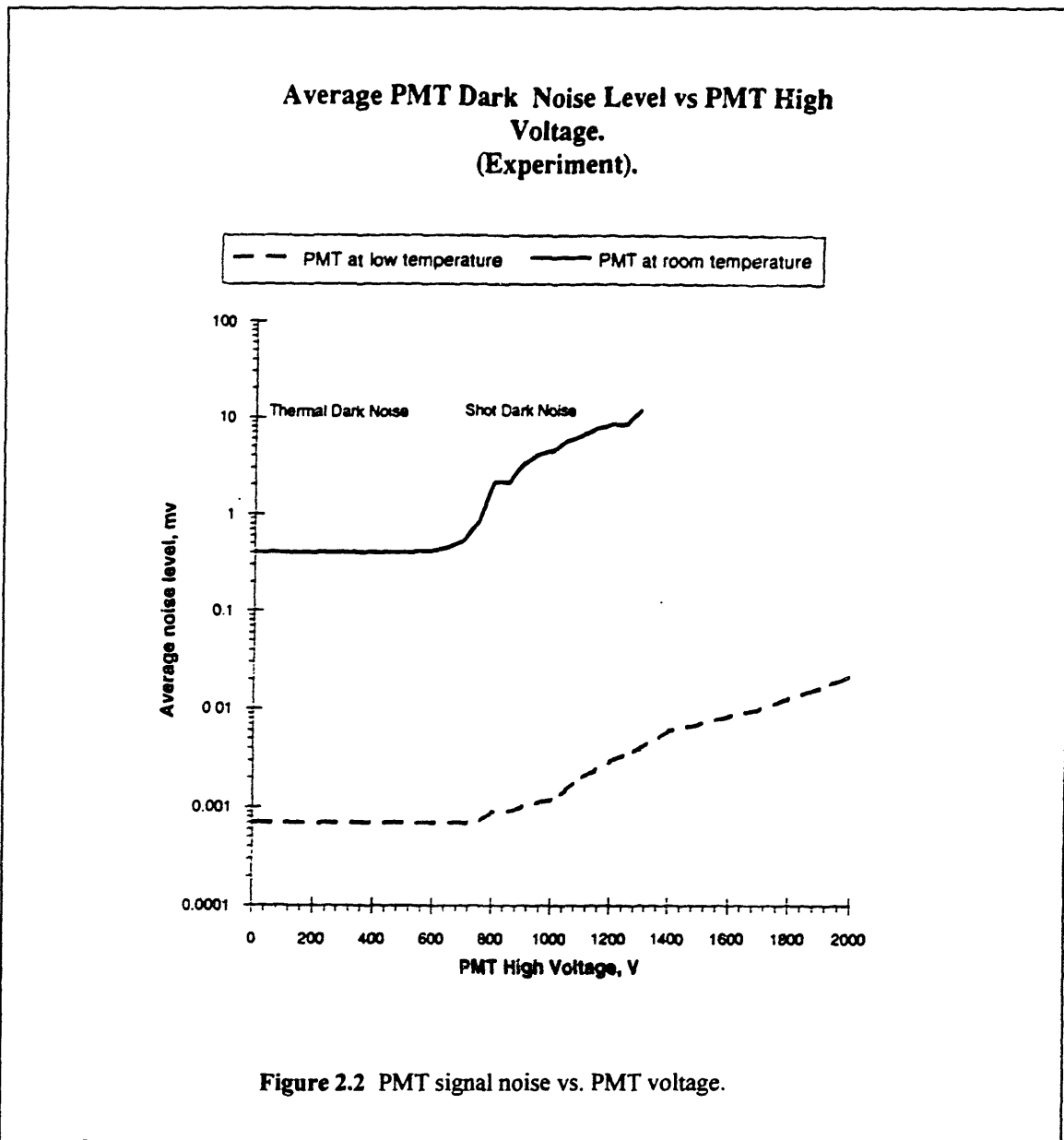
Figure 2.1 Schematic of Laser Induced Fluorescence System.

The focusing probe can be adjusted so that the laser beam is focused onto the oil layer on the cylinder liner, thereby maximizing the LIF signal-to-noise ratio. For these experiments, the laser focusing probe was adjusted so that the LIF signal on the oscilloscope was maximized. The portion of the signal which was maximized was the large masses of oil in the lands and skirt. It might be advantageous to investigate if it is possible to focus directly on the sub-ring oil films (1-4 microns) rather than focusing on the large oil masses (50-200 microns).

The engine oil is doped with a coumarin-based fluorescent dye which fluoresces at a wavelength of 495 nm when impinged upon by the laser beam. The oil's fluorescence intensity is linearly proportional to the oil film thickness until about 80 microns [5].

The fluorescence is carried out of the engine via a fiber optic cable which bifurcates from the original cable. The fluorescence is detected by a photo-multiplier tube (PMT) and a signal amplifier assembly which converts the oil fluorescence light intensity to a voltage that can be recorded by a data acquisition computer.

The PMT chosen for this LIF system was one which was tuned for maximum response in the 200 to 800 nm wavelength region. To ensure that only the oil fluorescence light reaches the PMT, a pair of 495 nm optical filters were installed in front of the PMT input. There is also a set of lenses in front of the PMT input which focuses the fluorescence light from the fiber optic cable to a 3.2 mm spot on the PMT.



The PMT input voltage setting is crucial to obtaining a strong LIF trace. The higher the PMT voltage, the stronger the LIF signal amplification. However, there are two reasons for imposing an upper limit on the PMT voltage. First, as shown in Figure 2.2, if the PMT voltage is set above about 700 volts, the PMT signal noise increases dramatically [6]. Second, the data acquisition system has a maximum voltage reading of 10 volts, so setting the PMT voltage such that the LIF signal on the oscilloscope reads greater than 10 volts will result in upper-bound signal saturation. An exception to the latter is if the experimentalist wishes to really focus in on

the minimum oil film thickness under the rings, and is not concerned with losing the macroscopic oil behavior on the piston lands and skirt.

As the engine oil temperature increases, the fluorescence efficiency of the oil mixture decreases. Therefore, to maintain a strong signal for the higher temperature data sets, the PMT voltage must be increased. Some typical PMT voltage numbers are: 580 volts for fired sets at 60 degrees C, and 680 volts for fired sets at 100 degrees C. The relationship between LIF signal and PMT voltage is of a very non-linear complicated nature and is described in [7].

Before the PMT output is recorded by the computer, the raw signal goes through a low-pass noise filter at 100 kHz. This cutoff frequency was determined by the most frequency-intensive case of running the engine at 3500 rpm, with a 4000 points/rev shaft encoder. Under these conditions, the maximum piston speed is approximately 12.5 m/s. The highest frequency feature of the piston assembly that we need to distinguish is the upper piston tool marks. The tool marks have a wavelength of about 0.3 mm, so at a piston speed of 12.5 m/s, the absolute minimum sampling frequency needed is 42 kHz. To prevent excessive signal aliasing, the Nyquist criterion [8] can be applied for a minimum sampling frequency of 84 kHz. A 100 kHz low-pass filter was chosen because it met the Nyquist criterion and was readily available in the laboratory.

Each component of the MIT LIF system is listed in Table 2.1.

<b>Component</b>	<b>Manufacturer</b>	<b>Part Number</b>
14 mW He-Cad laser, 442 nm and Power Supply	Liconix	4214 N
442 nm optical filter (2)	Oriel	52086, 1 inch OD
Filter Holder	Oriel	51594
Laser to Fiber Optic Cable Coupler (eccentric coupler)	General Fiber-Optic	85-22
Bifurcated Fiber Optic Cables	General Fiber-Optic	custom made for application
LIF Focusing Probe	LNS Machine Shop	custom made for application

Laser-to-Engine LIF Focusing Probe Lenses (2 per probe)	Oriel	41116
LIF Windows (fused quartz/silica)	Gould Precision Optics	custom made for application
<b>- Start of PMT Focusing Assembly. -</b>		
Oriel Fiber Input Flange	Oriel	77850
Flange Collar	Oriel	77829
Collar Coupler (male/male)	Oriel	78122
Optic Holder w/ lens holding collar. (1 of 3)	Oriel	7123
Lens (laser to PMT #1, focal length = 38mm, convex toward PMT.)	Oriel	41330
Optic Holder w/ lens holding collar. (2 of 3)	Oriel	7123
495 nm Optical Filter (2)	Omega Optical	495DF20
Optic Holder w/ lens holding collar. (3 of 3)	Oriel	7123
Lens (laser to PMT #2, focal length = 150mm, convex away from PMT.)	Oriel	41370
4 inch Spacer *	Oriel	7132
Collar Coupler (female/female)	Oriel	77829
PMT Housing *	Products for Research	custom made for application
<b>- End of PMT focusing assembly. -</b>		
Photo Multiplier Tube (PMT)	Hamamatsu	R4220
PMT Socket and Amplifier	Hamamatsu	C1053-01
High Voltage Power Supply for PMT	Bertan	230-03R

+/- 15 Volt Power Supply for PMT Amplifier	Newark Electronics	SLD-12-1010-12
100 kHz Low Pass Filter with BNC input and output	Sloan Electronics	custom made for application
Fluorescent Oil Coumarin Dye (5g)	Exciton	Coumarin 523
Data Acquisition System	Keithley Metrabyte	DAS-50

\* Modify "4 inch spacer" and design "PMT Housing" so that the distance from the flat side of 150 mm lens to the PMT face is 109.6 mm (4.315"). For the current system, a length of 34.92 mm (1.375") was machined off the "4 inch spacer."

**Table 2.1:** Components of the MIT LIF system.

## **2.2 THE ENGINE: KOHLER CH-14 SINGLE-CYLINDER SPARK IGNITION ENGINE WITH LIF WINDOWS**

The engine used for the LIF experiments was a Kohler CH-14 single-cylinder spark-ignition engine. General engine specifications are given in Table 2.2.

Engine	Kohler CH-14 single-cylinder spark-ignition. Cast aluminum block with iron cylinder liner.
Displacement	398 cc, bore x stroke = 87mm x 67mm.
Connecting Rod Length	112.9 mm
Power	10.5 kW @ 3600 rpm.
Torque	28.9 Nm @ 2600 rpm.
Cooling	Retrofitted water jacket around head, city water @ 4 degrees C.
LIF Windows	Six: four at midstroke, one near each endstroke on thrust side.
Pressure Transducer	Kistler 6051A with Kistler 503D amplifier, One mounted in cylinder head next to spark plug.

Thermocouples	Omega K-type, Two: one near top center on thrust side, and one near bottom center 90 deg. offset from thrust side (from top view).
---------------	--

**Table 2.2:** Kohler engine specifications.

The Kohler engine cylinder liner was machined for six LIF windows: four at midstroke, and one near each endstroke on the thrust side. The LIF windows were ground from a fused quartz/silica with a light transmission efficiency of over 90 % at the laser and fluorescence wavelengths. The locations of the windows is described in greater detail in Section 2.2.1. These windows are of the same design used by Deutsch [3].

Of the six windows, four windows were used for the LIF experiments. The top center window was not usable because of combustion residue build up over the window. Even after firing for a very short time (several minutes), a brownish ring of sludge built up on the upper region of the cylinder where the top ring does not scrape (top 5 mm of liner). Then, a lighter tinted ring about 6.5 mm wide formed just under the sludge. The center of the top center window was located right around the border of the thick sludge and the lighter one. The laser/fluorescence transmission efficiency was so poor that even at PMT voltages of well over the maximum recommended 700 volts yielded a signal which was barely legible on the oscilloscope.

The other inoperable window was the midstroke anti-thrust side window. The cause of this window's failure is still not completely understood, but could be due to a number of reasons. First, there was a slight oil leak from the engine cylinder, but this is believed to have been repaired (i.e. oil leak is no longer detectable). Second, there are a few visible scratches on the window surface inside the cylinder which may dramatically decrease the window transmission efficiency. Perhaps, the window got scored during the piston installation. Third, the laser focusing probe for the anti-thrust side window has to pass right next to the push rods of the valvetrain, and it is possible that the vibration from the rods reduces the LIF signal to a barely recognizable noisy hash. Yet another explanation may be the laser focusing probe design. The probe for this particular window is about twice as long as those for the other windows because of the extra length needed to get past the push rods. The drawings for the LIF probes and the engine block are given in [3].

The windows were installed such that they were very slightly recessed. A wooden anvil was lightly wedged inside the cylinder bore, pressing the window into the liner. At the same time, a soft-tipped threaded rod was screwed in from the outside of the cylinder to prevent the window from being overly recessed into the liner. The goal is to mount the window so that it is flush with the liner surface, or very slightly recessed (less than 25 microns (.001”), which can be felt by hand). The rationale for this is as follows: after the windows are installed, the liner has to be honed to ensure that the liner/window interface is as smooth as possible. Since the quartz window is harder than the iron liner, as the cylinder wears under the honing stones, a window that was protruding into the liner will end up protruding even more. If the windows were installed perfectly flush with the liner to begin with, honing would not be necessary.

Since the window bonding epoxy takes several hours to cure, the final adjustments of the window seating can be made by hand. When setting up for the honing procedure, it is important to check the Kohler maintenance manual for the maximum allowable bore diameter  $D_{max}$  for use with the standard piston and ring set. The cylinder was honed until the cross-hatch marks can be seen uniformly on both the liner and the window without exceeding  $D_{max}$ . If  $D_{max}$  is exceeded, a selection of over-sized pistons and ring sets are available from Kohler. The honing job was contracted out to Ideal Engine Rebuilders, Inc., in Somerville, MA.

During the honing procedure, as much of the engine was assembled as possible to simulate the residual bolt-tightening loads on the cylinder liner under normal engine use. To simulate the cylinder head load, a torque plate was fabricated out of a flat 12.7 mm (1/2”) aluminum plate. The plate had the five head bolt holes and a hole the size of the bore to allow easy access into the cylinder liner. In bore distortion measurements made by a simple micrometer, the torque plate made a difference as large as 35 microns (.0014”) near the top of the liner.

The Kohler engine was originally an air-cooled engine, with cooling fins cast into the upper engine block and around the entire cylinder head. For more precise temperature control over a wider temperature range, the engine block was retrofitted with a water jacket around the upper engine block fins. A 1.59 mm (1/16”) thick aluminum band was stitch welded on to the fins and the gaps were filled with an aluminum-based epoxy. As a test, an aluminum band was welded

onto an old Kohler block to check for bore distortion. The cylinder was stuffed with wet rags to prevent excessive heating of the block. During the welding of the aluminum band to the cooling fins, the block remained cool enough to comfortably touch by hand, so thermal distortion of the bore is assumed to be negligible.

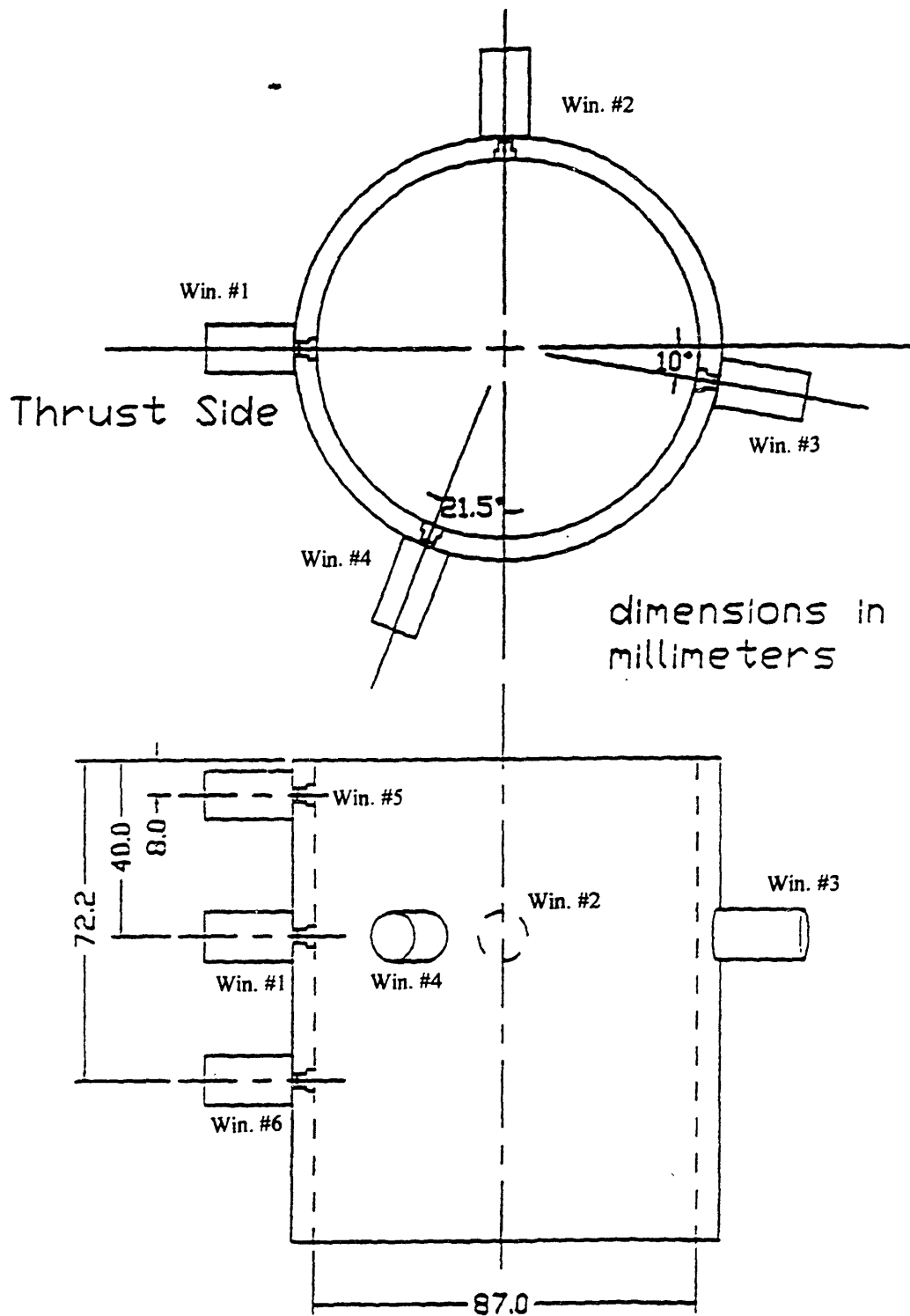


**Figure 2.3** LIF probe/window locations and window number convention of Kohler engine. (Deutsch Thesis [3])

### 2.2.1 LIF Window Locations

The Kohler engine used for this study is equipped with six quartz LIF windows: four placed circumferentially about 90 degrees apart at midstroke, one near top center on the thrust side, and one near bottom center also on the thrust side. A diagram of the window location is given in Figure 2.3 [3]. The purpose of the four windows at midstroke is to study the circumferential variation of the oil film thickness. Factors that could influence this circumferential variation include cylinder bore distortion, ring gap location, piston geometry, and piston secondary movement (piston tilt and piston slap).

The purpose of the windows near the endstrokes is to investigate the oil behavior under and around the piston rings during piston motion reversal. Also, the oil film thickness at the endstrokes can be compared to those at midstroke to study the trade off between high-speed midstroke friction and low-speed endstroke wear.

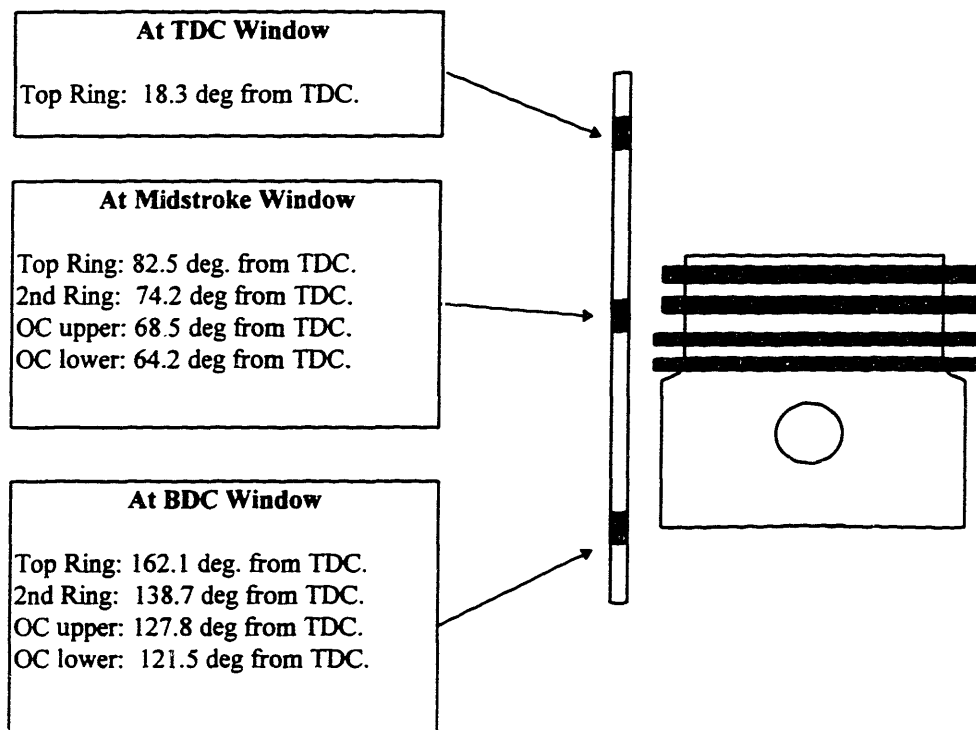


**Figure 2.4** Crank angle positions for each ring at each window location in the Kohler engine. Positions denote center of ring at center of window.

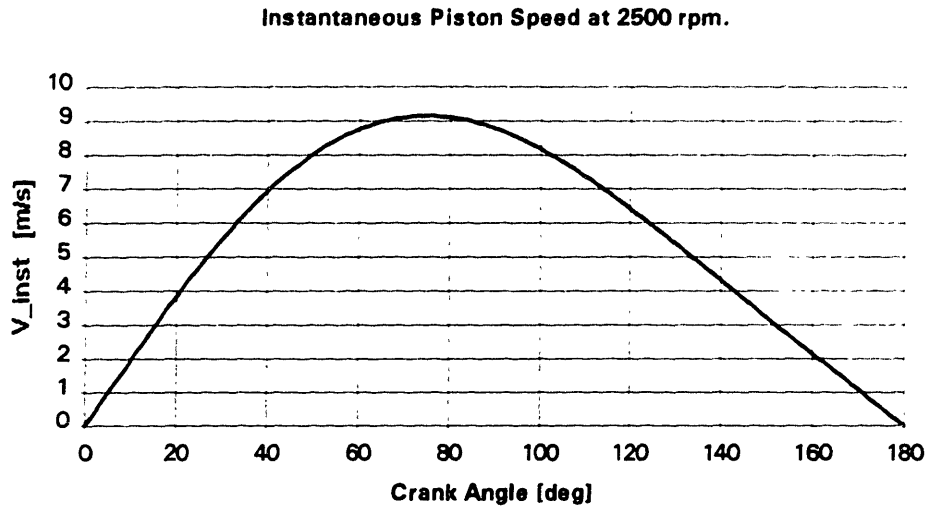


**Figure 2.5** Instantaneous piston speed vs. crank angle for Kohler engine at 2500 rpm.

When comparing oil film thicknesses of the endstrokes to those of the midstroke, it is very important to keep track of the ring velocity relative to the liner, of each ring at each window. As shown in Figure 2.4, at midstroke (all four windows at midstroke located at same cylinder height), all four rings pass the window at crank angles between about 64 and 83 degrees after top center. From Figure 2.5, we can see that the speeds of all four rings at the midstroke windows are within about 5% of one another at about 9 m/s. Therefore, a midstroke LIF graph like the one shown in Figure 2.6 can be thought of as a continuous set of ring profile snapshots that can be compared to one another. For example, at midstroke, the minimum oil film thickness under the lower oil control rail is greater than that under the top compression ring.

In contrast, the bottom center window sees the four rings pass by at very different speeds. By the time the piston has traveled far enough down that the top ring is at the bottom center window, the piston speed has dropped significantly. Notice from Figure 2.4 that the top ring passes by at 162.1 crank angle degrees after top center at a speed of about 2 m/s, significantly slower than its speed at the midstroke window of about 9 m/s. However, the lower OC rail passes by the bottom center window at 121.5 crank angle degrees at a speed of close to 6.5 m/s, which is comparable to its speed at midstroke of 9 m/s. What this means is that when examining an LIF data trace

from the bottom center window, as shown in Figure 2.7, we must keep in mind that the oil traces on different segments of the piston were created by those piston segments traveling at different speeds. A good indication of this is that the data points are closer together at the top ring region than they are at the higher speed OC rail region. This happens because the spatial sampling frequency (points per distance along piston) increases as the piston slows down, since the data acquisition is triggered by a constant 4000 points/rev encoder. Similarly, it is not valid to compare film thicknesses of the four rings recorded from the bottom center window to one another since film thickness is dependent on ring speed.

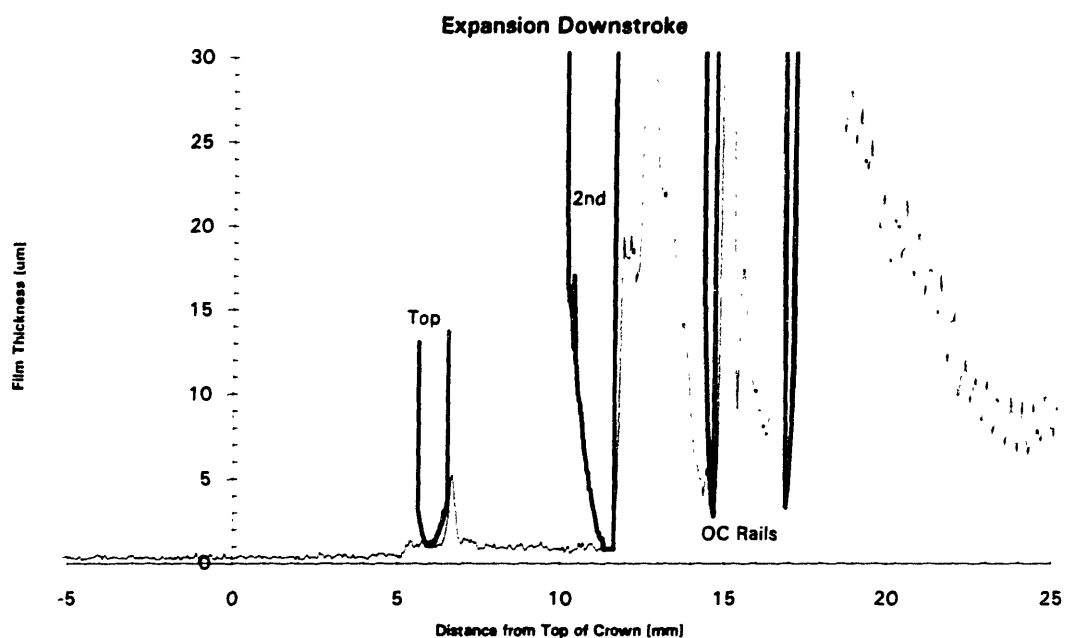


**Figure 2.6** Typical LIF midstroke trace.

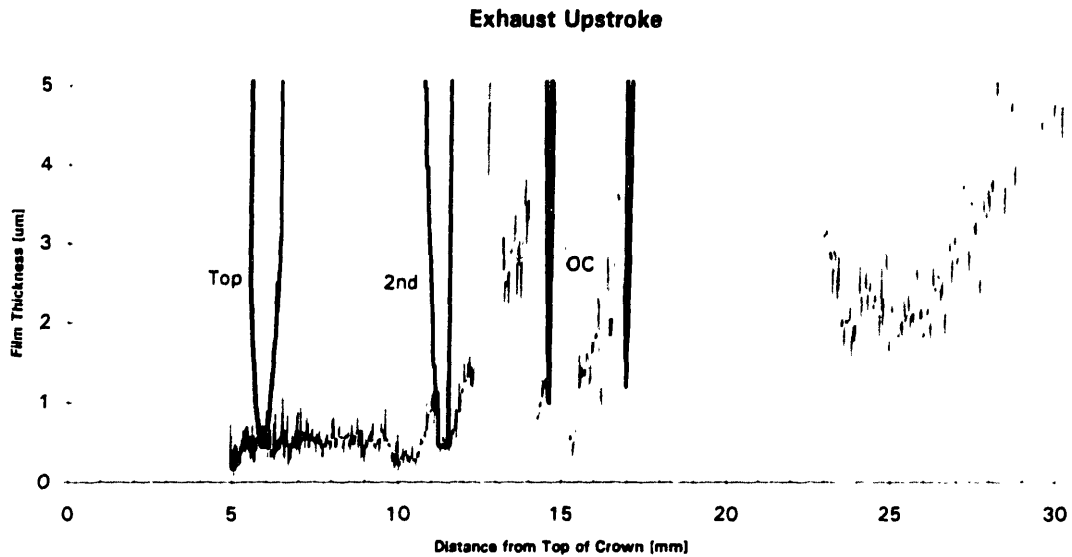


**Figure 2.7** LIF trace from the bottom center window (win. #6). Notice that the spatial sampling rate when window #6 sees the top of the piston (where piston velocity is low) is higher than that when the window sees the piston skirt.

### 2.2.2 Cylinder Liner Thermocouples

In order to monitor the temperature of the engine cylinder liner, the liner was fitted with two thermocouples. One thermocouple was installed near top center next to window #5 on the thrust side, and another was installed near bottom center approximately 90 degrees offset (clockwise in top view) from the thrust side. The temperature of the liner at midstroke is assumed to be the average of the temperatures at top center and bottom center. This assumption can be strengthened by holding the temperatures at top center and bottom center as close as possible. Careful control of the water jacket flow enabled the top center and bottom center liner temperatures to be held within about 5 degrees C of each other for all the operating conditions. To ensure that the temperature recorded by the thermocouple was as close as possible to that of the cylinder liner surface, the thermocouple tip was embedded approximately 60% through the iron cylinder liner.

Since the upper skirt region will be used for the LIF signal calibration, it is important to have the upper skirt temperature equal to the liner temperature. Two independent studies, one by Furuhamma et al [9] and the other by French et al [10], on two different engines, showed that the top center liner temperature is within 5 degrees C of the upper piston skirt region temperature. A summary of the temperature findings from the two papers are given in Table 2.3. This data shows that it may be reasonable to assume that the temperatures at the top center cylinder liner and at the upper skirt of the Kohler engine may be very close also. We have assumed that the LIF calibration constant obtained by referencing the upper skirt geometry is still valid when applied to the oil film on the top center cylinder liner, and on the rest of liner if the entire liner is held at the same temperature. This assumption is validated in Section 6.4.2 in which an alternate calibration method is used to produce a consistent calibration coefficient.

<b>Author</b>	<b>RPM</b>	<b>Intake Manifold Pressure</b>	<b>TOP CENTER Liner Temperature</b>	<b>BOTTOM CENTER Liner Temperature</b>	<b>Top of Skirt Temperature</b>	<b>Engine/ Cooling</b>
Furuhamma/ Enomoto	5000	.66 atm	<b>100 deg. C</b>	90 deg. C	<b>105 deg. C</b>	4 cyl, 1300 cc/ Water cooled
see above.	5500	.5 atm	<b>115 deg C</b>	100 deg. C	<b>120 deg. C</b>	see above.
French/ Atkins	5500	WOT	<b>130 deg. C</b>	not avail.	not avail.	4 cyl, 2000 cc / Water cooled.
see above.	6000	WOT	not avail.	not avail.	<b>130 deg. C</b>	see above.

**Table 2.3:** Engine component temperature data by Furuhamma et al, and French et al showing that top center cylinder temperature is very close to that of the upper piston skirt.

### 2.2.3 Cylinder Pressure Transducer

In order to monitor the engine cylinder pressure, a pressure transducer was mounted in the cylinder head next to the spark plug. Though the pressure vs. voltage output slope of the unit remains constant, the zero offset drifts from day to day. Therefore, when processing the

pressure data, the zero offset was determined by assuming the cylinder pressure during the exhaust stroke, before the intake valve opens, is equal to atmospheric pressure of 1 bar.

### **2.3 DATA ACQUISITION SYSTEM**

The data acquisition system used to acquire the LIF and cylinder pressure data was a DAS-50 unit from Keithley Metrabyte. The DAS-50 has 12 bit resolution, meaning if the voltage scale of the data were set at 0 to 10 volts, the DAS-50 would deliver a voltage resolution of  $2^{12}$  increments, or 0.00244 volt increments, across 10 volts. The DAS-50 was installed in a 486-33 MHz IBM-clone personal computer.

To start acquiring data, the DAS-50 is triggered by a 4000 points/rev shaft encoder mounted on the output shaft of the Kohler engine. However, this simple triggering could lead to some confusion since the encoder delivers a top center pulse every 360 crank angle degrees, whereas an engine cycle is 720 crank angle degrees. We need to make sure, at least for convenience, that each data set begins at the start of a common engine stroke. The encoder is mounted to the engine crank shaft so that the pulse coincides with the TOP CENTER position. How this alignment is accomplished is described in detail in Section 6.3 (Engine Kinematics). In order to distinguish between the beginning of the intake stroke and the beginning of the expansion stroke, a signal conditioner [4] which compares the pressure trace at the top center position of the two strokes was installed before the DAS-50. If the pressure is greater than a pre-set threshold, the signal conditioner erases the encoder pulse for that stroke. Therefore, what the data acquisition system sees is a top center trigger pulse every 720 crank angle degrees at the start of the intake stroke.

A concern when acquiring data is the sampling rate. We need to make sure that the physical details of the piston components are represented by a sufficient number of points. A 4000 points/rev sampling rate yields a spatial sampling resolution of 55 microns between each data point along the cylinder liner at midstroke. Therefore, an OC rail that is about 0.5 mm wide can be represented by nine data points. In the past, sufficiently detailing the OC rail oil behavior

was impossible because we only had a 2000 points/rev encoder which lead to gross signal aliasing.

Another aspect of the sampling rate that we need to be concerned with is the number of channels of data that we wish to acquire. The signal conditioner has the capability of acquiring up to four channels or "bursts" of data "simultaneously." Actually, each channel is acquired two micro-seconds apart. For this experiment, only two channels of data were recorded simultaneously: LIF and cylinder pressure. Therefore, with a 4000 points/rev encoder, and two channels (bursts) of data, the maximum speed that the engine can be run at before the bursts start overlapping is about 3750 rpm. Similarly, it is vital that the frequency response of the shaft encoder can also handle the engine operating condition. The encoder used for this experiment was manufacturer tested up to 2500 kHz which corresponds to a maximum engine speed of 3750 rpm.

## CHAPTER 3 TEST OILS

A set of five oils were tested. The set comprised of three mono-grade oils: SAE 10w, 30, 50, and two multi-grade 10w50 oils, one slightly thinner than the other. This study focuses on the SAE 10w, 50, and the thinner 10w50 oil. After all the experiments were run, the actual test oils were re-analyzed to assess whether the LIF dye or fuel contamination affected the oils' properties; they did not.

### 3.1 OIL VISCOSITY VS. TEMPERATURE

The Vogel equation [11] can be used to approximate the low-shear viscosities of the oils at temperatures other than those given by the oil supplier. Since the viscosity vs. temperature relationship is highly non-linear, performing a linear regression from two viscosity values at two temperatures is not valid.

The Vogel equation can be expressed as,

$$\eta = K \exp(\theta_1 / [\theta_2 + T]), \quad (3.1)$$

where,  $\eta$  is the kinematic viscosity in units of centi-Stokes (cSt),  $K$  is an oil-dependent constant in units of cSt,  $\theta_1$  and  $\theta_2$  are also oil-dependent constants but with units of degrees C, and finally,  $T$  is the temperature in degrees C at which the viscosity is being evaluated.

The results of the Vogel equation is shown in Figure 3.1 and Figure 3.2. The latter shows the same information as the former, except the viscosity axis is logarithmic to amplify the viscosity differences in the high temperature, low viscosity range. The high-shear viscosities were estimated to be 53% of the low-shear viscosities for the multi-grade oils at 100 degrees C [12].

Viscosity vs. Temperature for Multi and Mono-Grade Oils

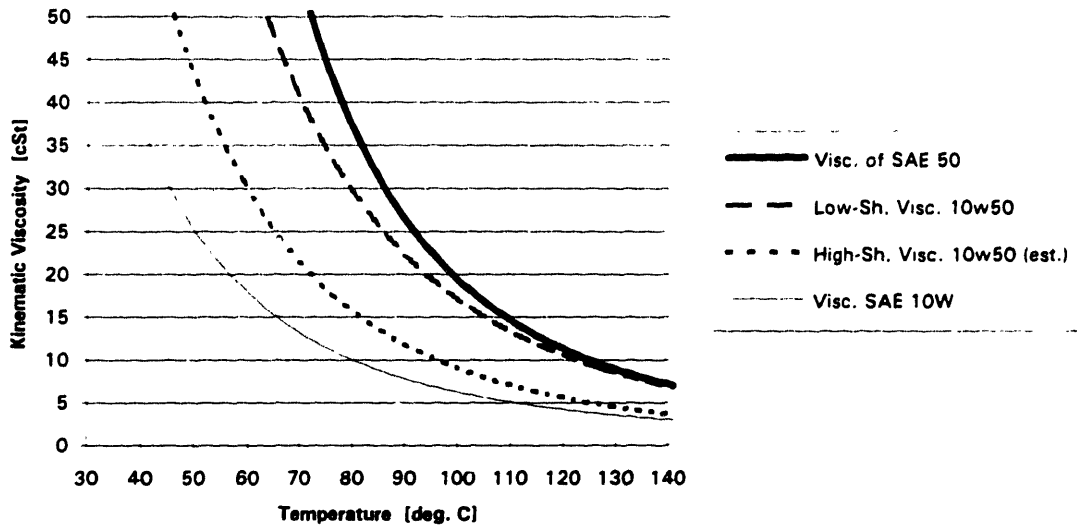


Figure 3.1 Viscosity vs. Temperature for multi and mono-grade oils. Notice non-linearity of viscosity trend.

Viscosity vs. Temperature for Multi and Mono-Grade Oils

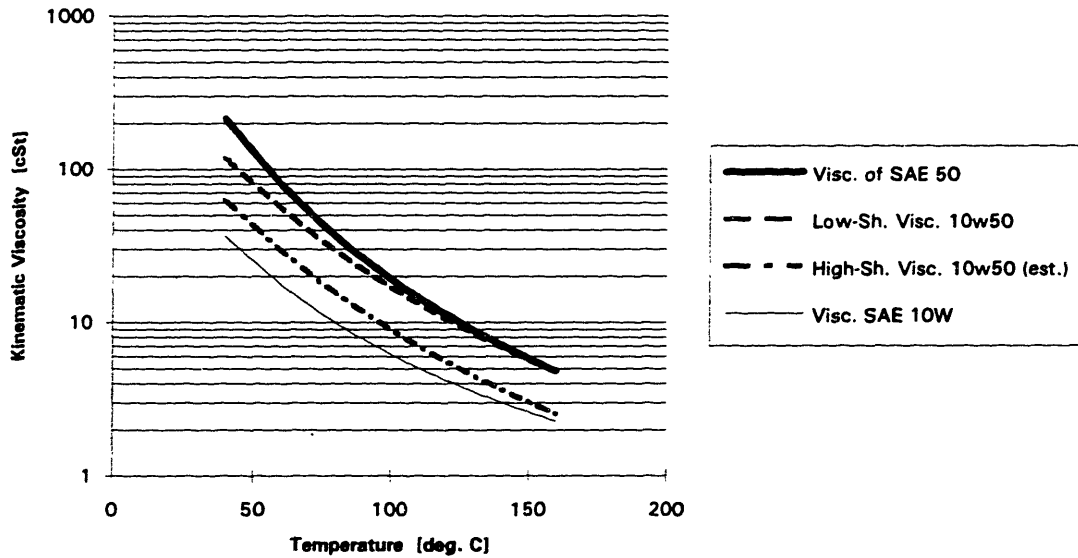


Figure 3.2 Viscosity vs. Temperature for multi and mono-grade oils on semilog scale.

Notice from Figure 3.1, the viscosity of the SAE 50 oil is roughly three times greater than that of the SAE 10w. With this large a viscosity difference, we should no doubt be able to detect a noticeable difference in the LIF measured film thickness. Also notice that the temperature drops more steeply at lower temperatures. For example, there is a bigger viscosity drop from 60 to 80 deg. C, than there is from 80 to 100 deg. C. Therefore, we expect a larger film thickness difference between the 60 and 80 deg. C cases than between the 80 and 100 deg. C cases.

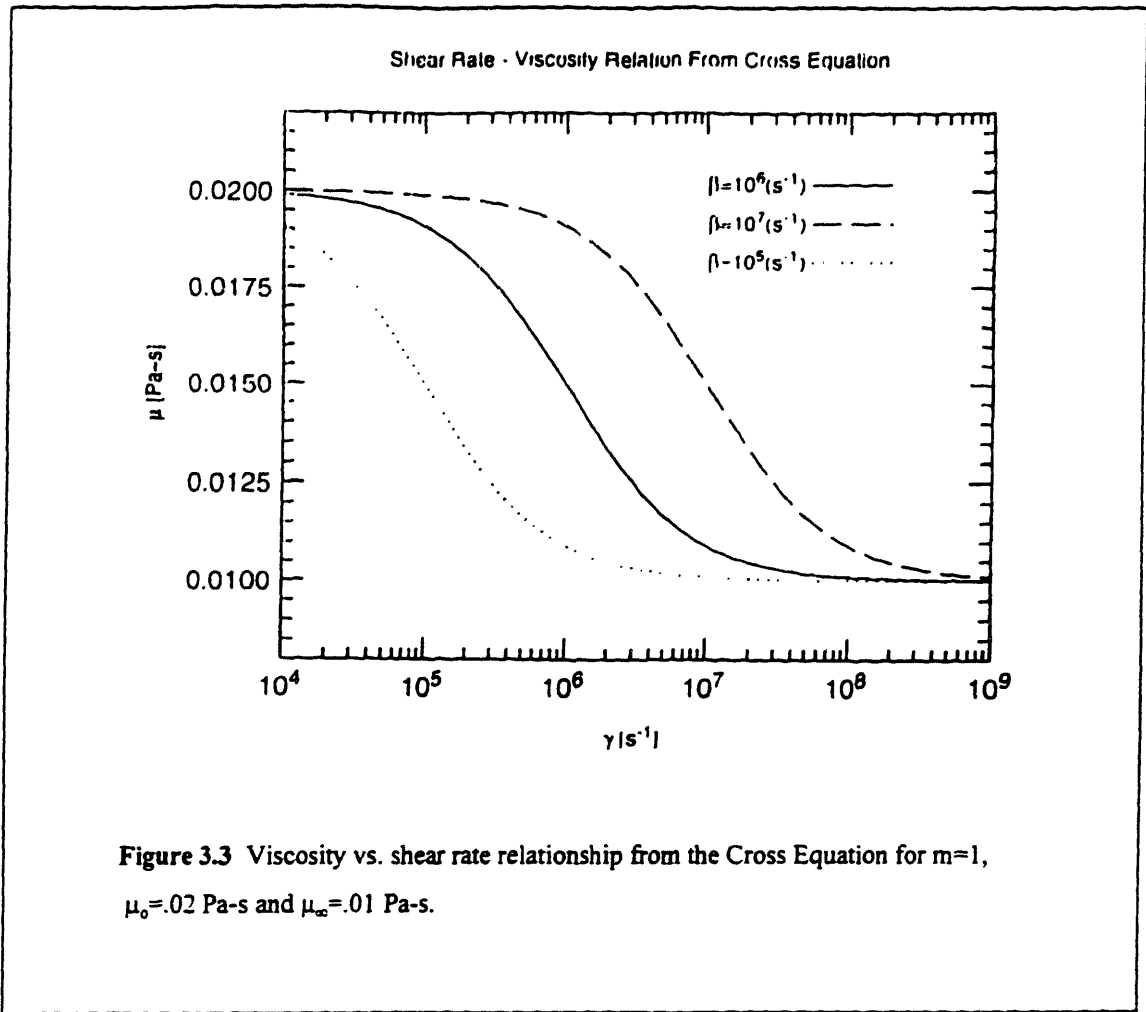
### 3.2 MONO-GRADE VS. MULTI-GRADE OILS

The main difference between multi-grade and mono-grade oils is that multi-grade oils have a less pronounced temperature vs. viscosity relationship [13]. Another difference between multi-grade and mono-grade oils is that mono-grade oils maintain a relatively constant viscosity even under extreme shear rates, whereas multi-grade oils undergo shear-thinning. A fluid which experiences no shear-thinning is known as a Newtonian fluid.

Shear-thinning is the change in viscosity as a function of shear rate, where shear rate is defined as  $du/dy$ . As shown in Figure 7.1, the  $u$  represents the oil flow velocity along the liner, and  $y$  represents the radial distance away from the cylinder liner.

A very simplified explanation of the shear-thinning effect is as follows. The low-shear viscosity represents the viscosity of the oil if it were simply sitting on the liner inside the engine cylinder. Then, if a piston ring were to slide across the puddle and shear across the fluid, a non-Newtonian fluid such as a multi-grade oil would undergo a decrease in viscosity if the sliding velocity reaches some critical speed. Figure 3.3 shows the plot of viscosity vs. shear rate for a 10w50 oil. An equation which expresses this shear-thinning behavior is the Cross Equation [14]:

$$\mu = \mu_o \frac{1 + \frac{\mu_\infty}{\mu_o} \left(\frac{\dot{\gamma}}{\beta}\right)^m}{1 + \left(\frac{\dot{\gamma}}{\beta}\right)^m}, \quad (3.2)$$



where,  $\mu$  is the viscosity at some shear rate  $\gamma$  (absolute value),  $\mu_0$  is low shear viscosity,  $\mu_\infty$  is the high shear viscosity,  $\beta$  is the critical shear rate, and  $m$  is a power constant.  $\beta$  is the shear rate in the middle of the transition region from the low-shear viscosity regime to the high-shear viscosity regime. The larger the power constant  $m$ , the narrower the transition region.

By convention, the viscosity values given by manufacturers are low-shear kinematic viscosities in units of centi-stokes (cSt). However, in a running engine, the oil between the cylinder liner and the piston rings are experiencing shear rates in the order of  $10^7$  1/sec; certainly in the high-shear viscosity regime. High-shear viscosity measurements can be made but the maximum feasible shear rate is approximately  $5 \times 10^6$  1/sec.

Shear-thinning is a desirable function of an engine oil because it helps to balance midstroke friction and endstroke wear. A reciprocating engine's piston travels at its maximum speed ( $\sim 10$  m/s) at midstroke, and slows down to 0 m/s at the endstrokes. At midstroke, the piston rings develop their greatest lift off the liner surface, and cylinder liner and piston ring wear is secondary to hydrodynamic friction. To minimize hydrodynamic friction at midstroke, oil viscosity should be low. However, at the endstrokes where the piston velocity is very low, the piston rings do not develop much lift and boundary lubrication can occur. In this case, engine liner and ring wear is a major concern, so a high viscosity oil which could statically support the ring by the squeeze effect (Section 7.14) is favorable. The hydrodynamics of ring lubrication is described in greater detail in Section 7.1.

A major goal of the multi-grade oil designer is to formulate an oil which could offer the engine the proper high-viscosity lubrication at the low-shear endstroke region, and then shear-thin to the proper low viscosity in the high-shear midstroke region.

## CHAPTER 4 TEST MATRIX

The experimental test matrix was designed to investigate the temperature and speed effect on a set of test oils. Each running case was repeated for each of the four operational LIF windows. With the data collected from the test matrix, film thicknesses from the different oils and different windows can be analyzed to deduce oil property, running condition, and liner location trends.

The baseline running condition was chosen to be: fired at 2500 rpm, 20 Nm torque (bmep = 631 kPa), and a midstroke liner temperature of 100 deg. C. The above engine speed and torque was chosen because the engine and dynamometer ran most smoothly and consistently at that running condition. Perhaps with a more precise throttle control, lower torque setting could have been chosen. The baseline temperature of 100 deg. C was chosen to best simulate an engine in field use. Also, 100 deg. C is a convenient temperature because oil properties are often measured at this temperature. A flow chart of the test matrix is shown in Figure 4.1.

# Test Matrix

## Oil Film Thickness Dependence on Cylinder Liner Location and Oil Properties

February 1995

Kohler Single-Cylinder Internal Combustion Engine. Bore x Stroke = 87 mm x 67 mm.  
 LIF windows: Three circumferential locations at midstroke, one at bottom center on thrust side.  
 (Top-center window operational for motored conditions only due to combustion residue build-up.)

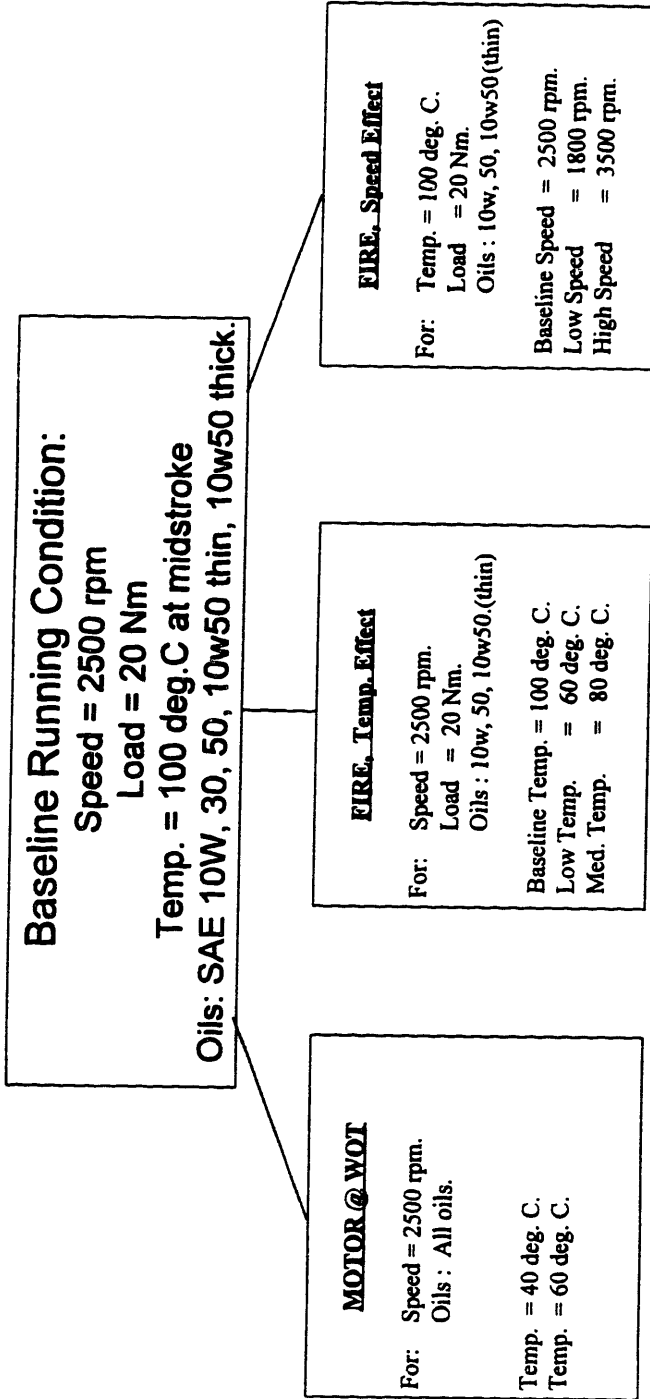


Figure 4.1 Test matrix for multi LIF probe Kohler engine.

## **CHAPTER 5 MICRO-MEASUREMENT OF ENGINE COMPONENTS**

A Talysurf profilometer machine was used to obtain the micro-geometry of the cylinder liner, piston machining marks, and piston rings. The machine is a tactile sensing instrument which makes use of a sharply pointed stylus to trace surface irregularities. The stylus used to trace the Kohler engine components had a tip radius of about 10 microns (.0004") and an included angle of 60 degrees. In addition to surface measurements, bore distortion measurements were done on the cylinder bore. Similar to the Talysurf machine, the roundness measuring machine also uses a stylus to circumferentially trace the inside of the cylinder liner.

The regions of the engine that were micro-measured before and after the experiments are:

- 1) Bore distortion at the three heights along the cylinder axis, corresponding to the window locations.
- 2) Window-to-liner flushness at all six windows.
- 3) Top ring face profile at three circumferential locations.
- 4) Second ring face profile at three circumferential locations.
- 5) Oil Control Rail face and side profiles at three circumferential locations.
- 6) Piston Skirt: thrust, anti-thrust, and side skirt (along axis of wrist pin) machining mark profiles.
- 7) Items (3) -(5) above for brand new rings.
- 8) Top land machining mark profile on thrust side.

The engine parts were first Talysurf<sup>ed</sup> after about 20 hours of initial break in. Approximately 50 hours of tests were performed before the current series of tests. The final micro-measurements were done after the experiments. Therefore, we can assume that the final Talysurf measurements are representative of the engine condition during the latest series of tests.

### **5.1 ENGINE BLOCK MICRO-GEOMETRY**

The following micro-measurements were made on various parts of the Kohler engine block after the test matrix was completed. Just as in the cylinder liner honing procedure, as much of the engine was assembled as possible to simulate the residual loads on the engine structure during normal operation. (Section 2.2). However, all the measurements were done at room temperature. At engine running temperatures of 100 deg. C, thermal deformations are inevitable, especially bore distortion, but there was no method available to make the measurements of the components in their heated condition. From an order of magnitude analysis using a linear thermal expansion coefficient of  $10 \times 10^{-6} \text{ 1/K}$  [13], we can assume that the dimensional change of the piston rings

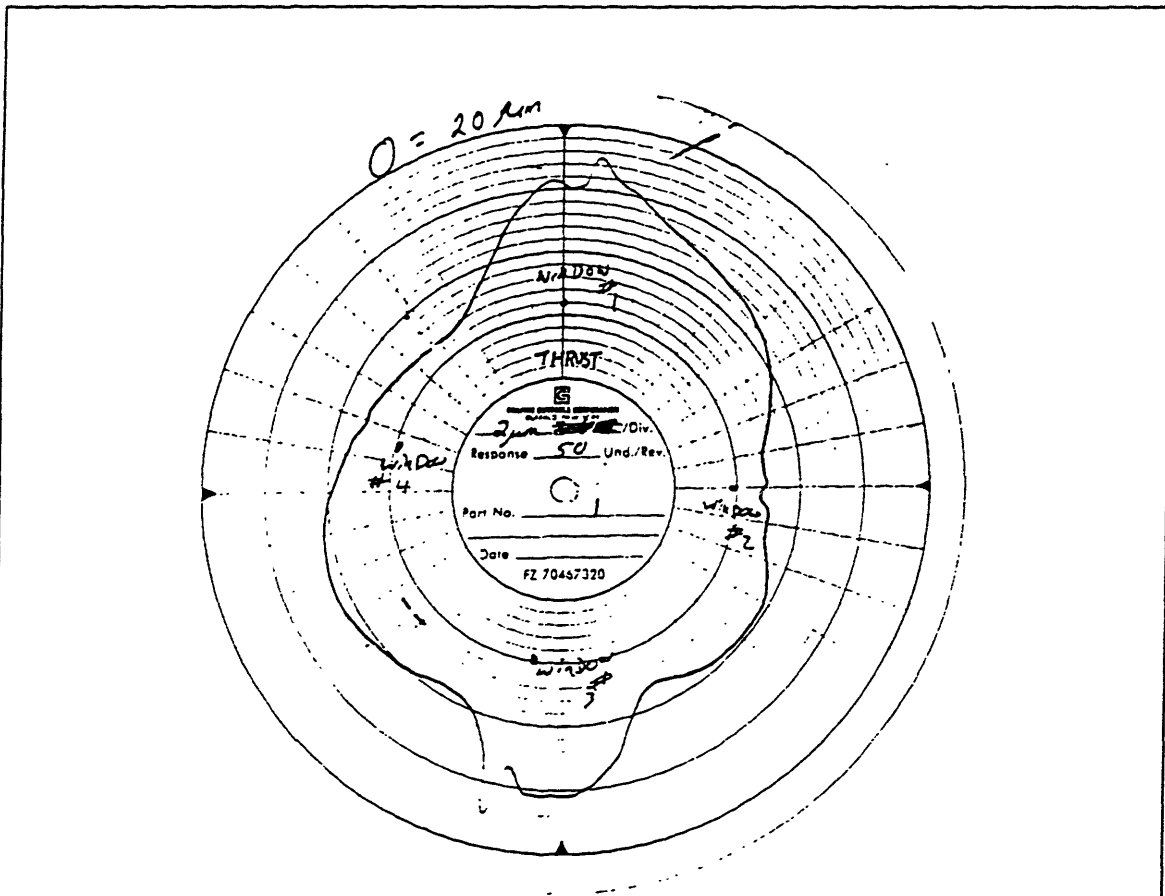
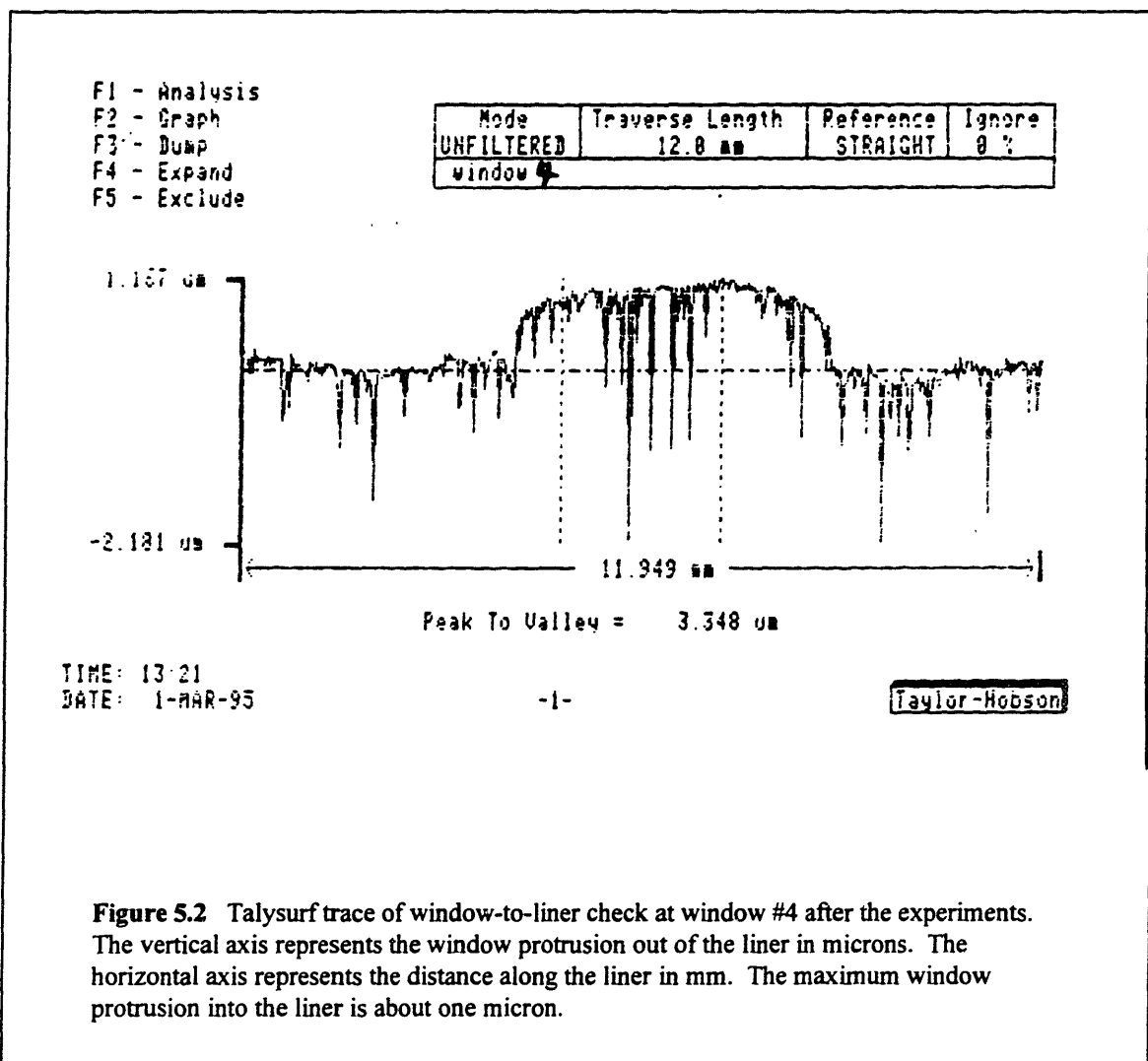


**Figure 5.1** Bore distortion plot at midstroke. Scale = 2 microns per division, maximum radial difference = 20 microns, max radial difference between windows = 16 microns (window #1 vs. window #2).

and skirt are negligible. However it is difficult to say the same for the engine block which has large temperature gradients and a much more complicated shape. Therefore, the bore distortion plots are used to give us a qualitative picture of which region of the liner is more worn than

another. The bore distortion plot at midstroke measured after the experiments is shown in Figure 5.1.

A Talysurf profilometer was used to measure the window-to-liner flushness of all six windows. Again, since the measurements were made at room temperature, and since the cylinder liner (cast iron), the LIF window (quartz), and the window glue all have different thermal expansion coefficients, the actual window-to-liner flushness under normal engine running conditions of 100 deg. C is only approximated. A print out from the Talysurf profilometer of one of the midstroke windows (win. #4) is shown in Figure 5.2. Notice the window protrudes into the cylinder about 1 micron. The window flushness of all the other windows after the experiments were



comparable to that of window #4; they all protruded out of the liner by 0.5 to 2.7 microns. In the Talysurf measurements made just after honing (before experiments), the windows were either

flush, or slightly recessed a maximum of about 0.7 microns. This recess is probably not a concern since the engine was run over 50 hours between the honing and the start of this test matrix.

The case of the slightly protruding window during experiments is definitely favorable to the recessed window case because a small protrusion of the window would still ensure hydrodynamic lift of the rings. However, a recessed window may not allow the ring face to touch the window at all, and the LIF oil film thickness measured would simply be that of the oil puddle sitting on the window. A concern with the protruding window is the ring tension difference due to the added deflection. However, the ring tension change due to a window protrusion of 1 micron is negligible for a typical ring tension rate in the order of 200 N/m [15].

## **5.2 PISTON AND PISTON RING MICRO-GEOMETRY**

The Talysurf tracing of the piston skirt machining marks and the top two piston rings were very straightforward. The rings were traced in three circumferential locations to check that ring rotation would not effect the ring fit in an LIF oil trace (exception would be if the ring gap fell on the window location). The ring profiles at the three locations for each ring were remarkably consistent. The representative top and second rings are shown in Figures 5.3 and 5.4, respectively. The piston skirt machining marks used for the LIF calibration is shown in Figure 5.5.

It is important to note that the piston upper skirt machining marks on the thrust side were of the same pitch and amplitude as those on the other circumferential skirt segments on the piston. The only exception is that no skirt exists at the circumferential location corresponding to window #4 (68.5 degrees counter-clockwise from the thrust side in top view), which happens to be the location of the OC rail expander drain port. Also notice in Figure 5.5 that the machining marks near the very top of the skirt have experienced some wear. If these worn teeth need to be used for LIF calibration, the slope of the teeth should be used rather than the amplitude because it is not certain what the condition of the machining marks were at the time of the experiment.

Kohler Top Ring 1995 Talysurf

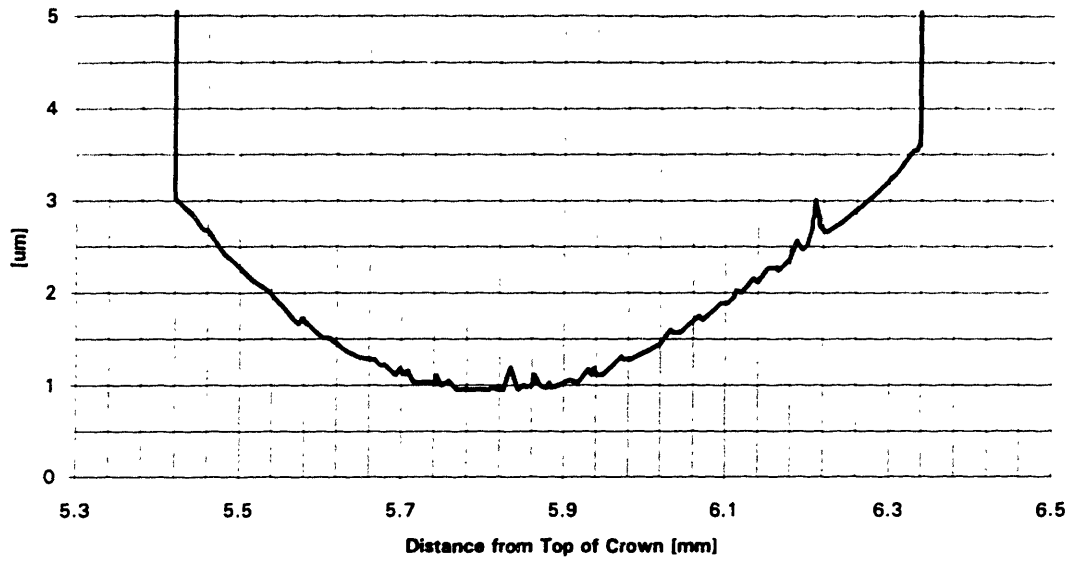


Figure 5.3 Talysurf of Kohler top ring.

Kohler 2nd Ring 1995 Talysurf

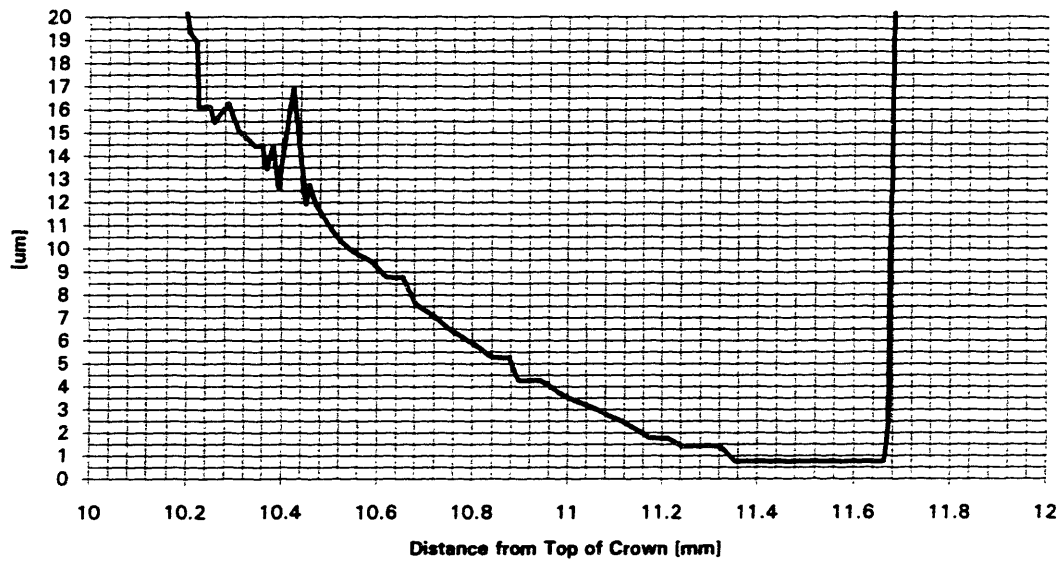
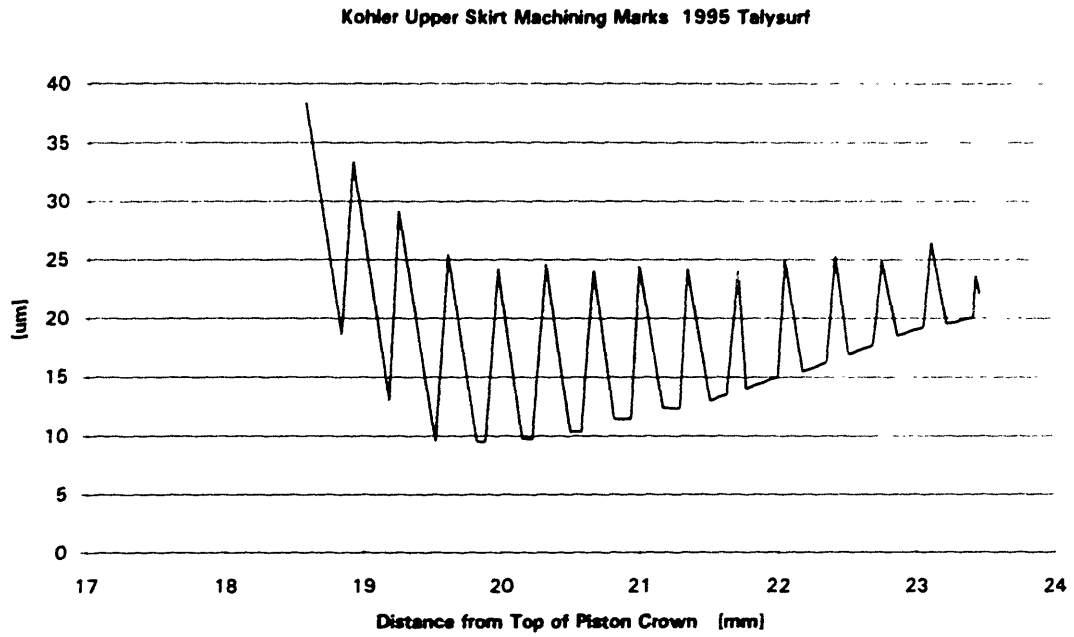
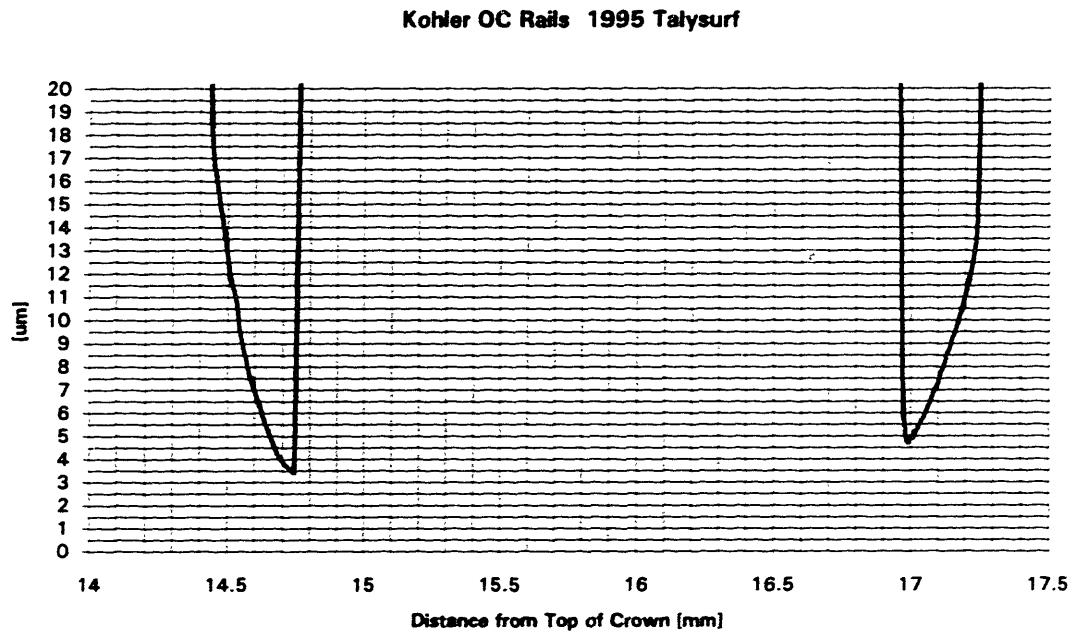


Figure 5.4 Talysurf of Kohler second ring.



**Figure 5.5** Talysurf of Kohler upper skirt machining marks.



**Figure 5.6** Talysurf of Kohler oil control rails.

The Talysurf tracing of the OC rails was much more difficult to obtain than those of the other engine components. Due to the very thin profile (half the width of the top two rings) and the relatively steeper slope of the OC rail faces, the stylus cone ended up hitting the OC rail and forced the stylus tip to lose contact with the rail surface. Therefore, the rail face and the two sides of the rail had to be traced separately. The rail face was traced with the OC rail clamped standing on its end, and the rail sides were traced with the rail clamped sitting flat on the Talysurf table. The three traces were then combined to construct an OC rail composite profile. The upper OC rail profile used for the LIF calibration and the lower OC rail profile are shown in Figure 5.6.

## CHAPTER 6 DATA PROCESSING

### 6.1 RAW LIF TRACE

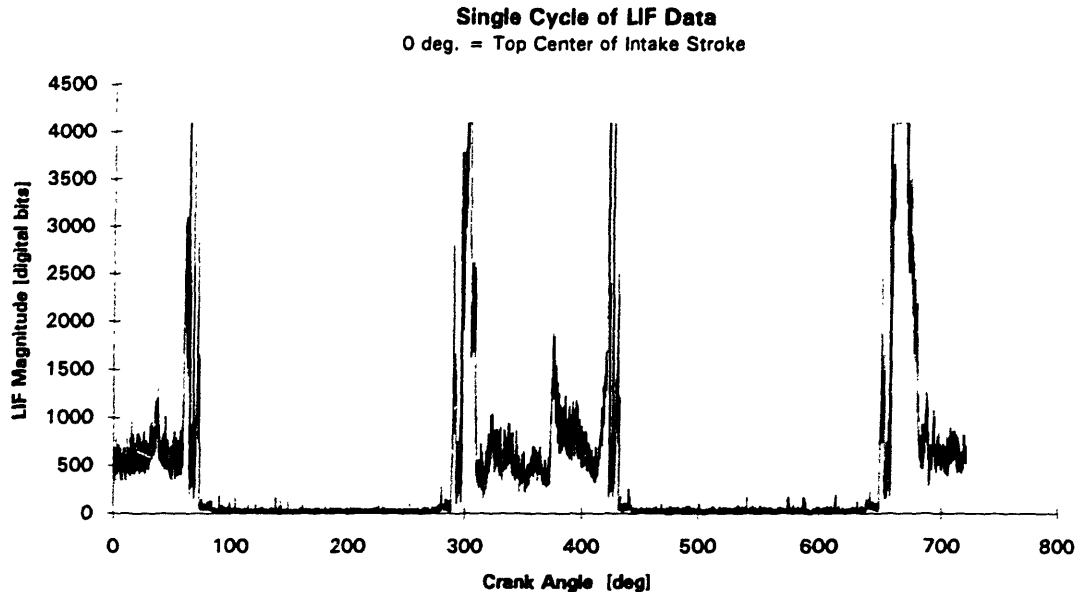


Figure 6.1 Full cycle of LIF data starting from the beginning of the intake stroke.

A typical single cycle of a raw LIF data file is shown in Figure 6.1. This particular trace was taken from the midstroke, thrust side window (window #1). The data set starts at the beginning of the intake downstroke. The first data points, starting from left side of graph, show the oil on the piston skirt. As the piston travels down the cylinder, the OC rails (large spikes) pass by the window followed by the second ring and the top ring. After the piston crown passes the window, the window sees nothing but the layer of oil left behind by the top ring. This layer of oil is the “free-liner oil film thickness” or the  $h_{\infty}$ . At the 180 crank angle degree point, the piston reverses its direction of motion. On the compression upstroke, the window first sees the free-liner oil film, followed by the piston top land, and the piston rings starting with the top ring. Once the rings have passed, the window again sees the piston skirt. After about 80% of the skirt has passed the window, the piston reverses its direction of motion and the expansion stroke starts. The LIF trace of the expansion stroke is graphically a mirror image of the compression

stroke. After the expansion downstroke, the exhaust stroke starts where the window first sees the free-liner film thickness followed by the piston top land and the rings.

## **6.2 ZERO OFFSET**

To determine the zero offsets of the LIF data sets, the engine and LIF system were run as if a typical data set were to be taken, except the laser input into the engine was disconnected and plugged off with a black rubber stop. A medley of tests were done varying the PMT voltage and engine speed. The zero offset was rather constant for all the tests at  $5.5 \pm 0.3$  mv. This variance of the zero offset would represent an oil film thickness of 0.004 microns (for a typical LIF calibration constant of 75 mv/micron).

When determining the LIF zero offset, there is some concern about random reflections from the piston and rings that may be picked up by the PMT which may contribute to the zero offset. A suggestion that has been made in the past is to flush the engine of the dyed oil and record LIF data to obtain the zero offset. However, flushing the engine of all fluorescent dye would be very difficult to do and evaluate. Also, since the optical filters in front of the PMT allow only the fluorescence wavelength of 495 nm to pass through, the amount of light reflected off the piston and rings, which would still be at the laser wavelength of 442 nm, that the PMT would detect would be negligible.

## **6.3 ENGINE KINEMATICS**

When processing the LIF data, it is very convenient to convert the x-axis from crank angle to “distance from top of piston crown.” This axis transformation enables easy placement of the piston and rings to the LIF trace, and thus facilitates the LIF calibration procedure.

In order to perform this transformation, we first need to understand the kinematics of the engine piston assembly and obtain precise geometric dimensions of the engine components. Since the geometric values given in the Kohler service manuals are only nominal values, the actual

components of the test engine such as the connecting rod, crank radius, distance from the top of liner to the crank axis, and the piston dimensions had to be measured. It is very crucial to measure the components very carefully since the resulting slopes of the LIF oil film trace can change. A measurement error of 0.5 mm (0.02") can cause errors as high as 1 mm along the distance on the piston. A schematic of the engine assembly is shown in Figure 6.2.

When performing the x-axis transformation, the kinematic analysis assumes that the first data point represents the top center crank angle position, so it is crucial to know precisely where the top center position is with respect to the data acquisition system (DAS) trigger. As described in Section 2.3, the DAS trigger defines where the data set starts being acquired. The relative positioning of the DAS trigger pulse (encoder pulse) and the top center position of the engine can be made by adjusting the encoder shaft position relative to the engine output shaft. There are a number of methods by which this alignment can be accomplished.

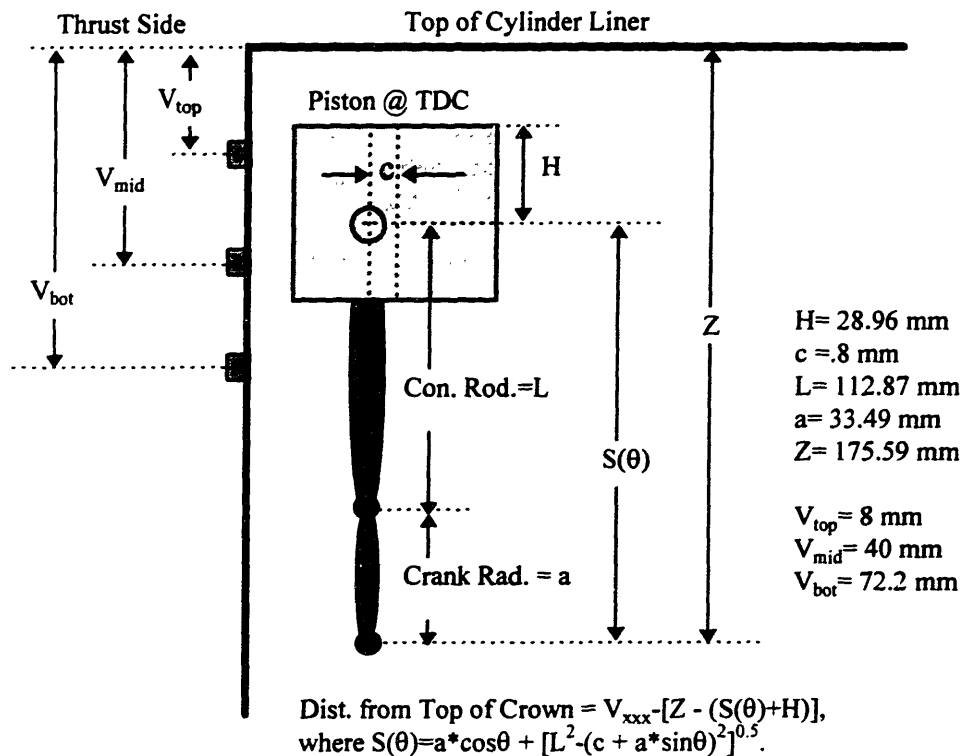


Figure 6.2 Schematic of Kohler piston assembly.

One method is to examine the motored pressure trace and assume that the pressure peak under motored conditions should occur exactly at top center. The adjustment can be made by observing the pressure trace and the trigger pulse on the oscilloscope, and turning the encoder like one would a distributor when adjusting spark timing. The alignment can be checked by recording the pressure trace along with the DAS trigger pulse and examining the data file to see that the pulse is located at the peak pressure location.

Another method of aligning the top center position and the DAS trigger pulse is to remove the engine head, and connect the encoder output to an oscilloscope. If the encoder is properly adjusted, a pulse should be visible on the oscilloscope when the crank shaft is manually turned so that the piston is in its top center position. This method proved to be useful only in determining whether the pulse came before or after top center. Measuring the piston position relative to the top of the engine liner and calculating what the crank angle was when the encoder pulse triggered was very difficult to do because at the dead center position, the piston barely moves even for several degrees of crank rotation.

The third method is to plot the LIF data on a graph which has piston distance on the x-axis as described in the beginning of this section (or as shown in Figure 2.6). By trial and error, the number of data points from the beginning of the data file that needs to be discarded or added can be determined by loading the modified data file into a spread sheet and seeing if the peaks and valleys of the LIF trace fall on the proper piston location. For example, we can check to see that the OC rail traces fall where the OC rails are geometrically located on piston.

All three of the above methods were used to process the data sets. Though this may seem somewhat labor intensive, it needs to be done only once given that the shaft encoder is never re-adjusted throughout the data taking period. For this experiment, the motored pressure peak method proved to be dead-on.

As a side note, the LIF trace of the intake stroke from window #1 (midstroke, thrust side) seemed to be shifted such that the oil trace ends up about 0.5 mm higher on the piston than calculated. Deutsch also consistently saw this [3]. The reasons given by Deutsch was that due to the low cylinder pressure during the intake stroke, the piston may get sucked up and all slop in engine

components stack up to result in the 0.5 mm shift. What is peculiar, however, is that the slop does not appear to stack up consistently in the opposite direction during the compression stroke. Another possible reason cited by Deutsch is piston tilt. A possible answer may be a combination of both effects because for this round of LIF data, the intake stroke shifts of windows #2 and #4 were about half of that of window #1. If the anti-thrust side window were operational, we can possible answer this question for sure. For the other three strokes, the offset of the LIF oil trace vs. the piston was typically .05 mm, which could easily be due to ring flutter within the ring groove, or bearing slop. Occasionally, the expansion stroke showed a shift of about -0.3 mm (opposite direction relative to intake stroke shift).

## **6.4 LIF OIL FILM CALIBRATION**

The purpose of the oil film calibration procedure is to convert the voltage signal from the PMT into a meaningful oil film thickness, usually in units of microns. The data sets from the midstroke windows and the bottom center window was calibrated using two back to back in-situ calibration methods: the piston skirt machining mark method and the upper OC rail method. Only single traces, as opposed to averaged traces, were used when performing calibrations. If there are cycle to cycle variations in the oil film behavior on the piston skirt or around the OC rails, the resulting averaged trace will not represent the actual wetting behavior. Possible use of bench experiments to determine LIF calibration coefficients are discussed in Section 6.4.4. For the MIT experiments, only in-situ calibrations were performed. Each data set was separately calibrated - a very time consuming procedure, but one which ensures that each data set is properly calibrated. The calibration coefficients of the processed LIF data is tabulated in Appendix C.

### **6.4.1 Piston Skirt Machining Mark Calibration Method**

In the past, as described by Deutsch [3], the most reliable method of LIF oil film calibration has been to use the upper skirt machining marks. These tool marks are often flooded with oil, and

since the piston skirt is barrel shaped, the upper most tool marks do not contact the cylinder liner, and thus do not wear. As shown in Figure 5.5, the top four or five machining mark peaks have not worn even after close to 100 hours of engine use.

The LIF trace first needs to be plotted with the “distance along from top of piston crown” as the x-axis. The Talysurf of the piston machining marks can then be superimposed on the LIF trace at its physical location along the piston length. The goal of the calibration procedure is to align the machining marks’ amplitude and slopes to the oil trace by iteratively adjusting the volts-to-micron conversion factor (trail calibration coefficient), until a match is found. An example of a good calibration fit is shown in Figure 6.3. Notice that about four teeth profiles match in amplitude and slope. The minimum of four teeth are usually used for determining a calibration constant.

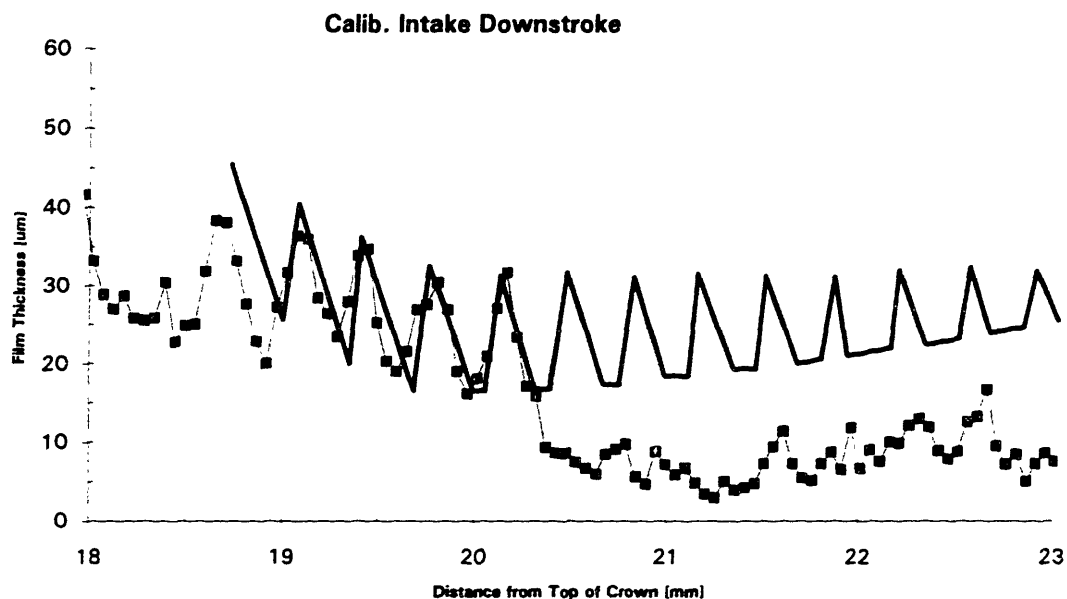


**Figure 6.3** Calibration of LIF signal by matching a segment of an LIF trace to upper-skirt machining marks.

The upper-skirt machining mark method has been successful, but some short-comings of the method include:

- 1) For some data sets, none of the cycles show flooded upper-skirt machining marks - must discard data set.

- 2) Time consuming to look for flooded machining marks.
- 3) Calibration coefficient is sometimes not very precise due to signal noise and insufficient wetting so, it is difficult to distinguish 30 mv/micron from 35 mv/micron.
- 4) Can only calibrate LIF signal where skirt is present. For example, for the LIF windows located along the piston wrist pin axis, no sufficient skirt exists from which to calibrate. Only if the laser transmission efficiencies through the quartz window and optical hardware are identical, can a calibration coefficient from another window be used. It may be possible to resort to machining marks on the second or third land for calibration, but no tool mark traces were seen in those regions in this particular engine.
- 5) If the upper skirt region is overly flooded with oil ( $> 80$  micron), the calibration coefficient is very questionable because of the LIF signal vs. oil film thickness nonlinearity discussed in Section 2.1.
- 6) Temperature of the piston skirt needs to be very close to that of the liner because fluorescence efficiency varies with temperature. However, this probably is not an issue as discussed in Section 2.2.2.

#### **6.4.2 Oil Control Rail Calibration Method**

An alternative calibration method is to use the slope of the OC rail face. This method requires the use of the OC rail Talysurf profile as the geometric reference to calibrate the LIF signal. Some advantages of this method include:

- 1) Wedge face of OC rails do not wear. Even if tip of the rail wears, wedge slope is still preserved.
- 2) The calibration site and oil film thickness measurement site are closer together than in the skirt method, so uncertainties such as temperature differences and LIF nonlinearity effects are minimized.
- 3) It may be possible to automate this procedure in the future. Unlike with the skirt mark method whose oil wetting is not guaranteed, the OC rail wetting is consistent. Automation of the LIF calibration procedure would cut the data analysis time tremendously since currently over three-quarters of data processing time is spent determining the calibration coefficient for each data set.

4) Calibration coefficient is very precise. The difference between 35 mv/micron and 40 mv/micron is often detectable.

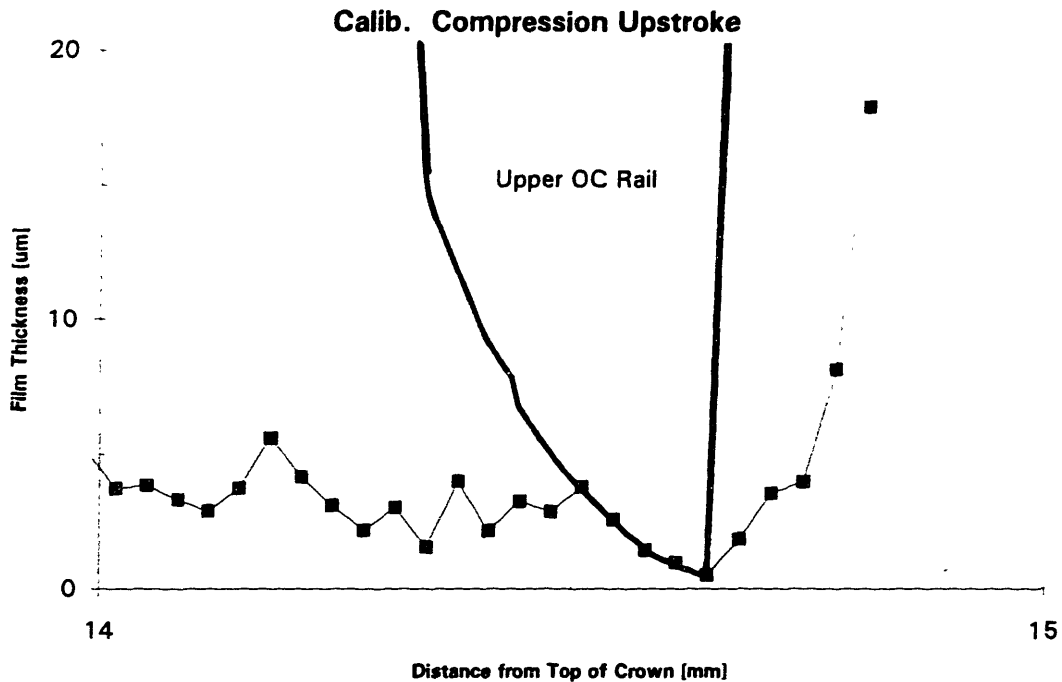


Figure 6.4 Upper OC rail fit into LIF trace for signal calibration.

The best OC rail wetting fits were found on the upstroke for the upper OC rail. An example of an OC rail fit is shown in Figure 6.4. Notice that there are five points across the slope of the wedge. Four or five points fitting across the OC rail for a calibration was quite typical. The minimum allowable number of points across the OC rail during a calibration was three, and that was only if they conformed very well to the OC rail contour. A plot which shows both the OC rails and the piston skirt fitted to a LIF oil trace for calibration is shown in Figure 6.5.

The lower OC rail was not useful for calibration probably because of over flooding by the large oil volumes on either side of the rail. The width of the laser beam impinging on the oil layer is about 50 microns [3]. If the slope of the OC rail side wall becomes increasingly steep from the wedge to the side wall, the fluorescence emitted by the oil volume sampled by the laser will not be representative of the oil film thickness at the center of the laser beam. Figure 6.6 illustrates

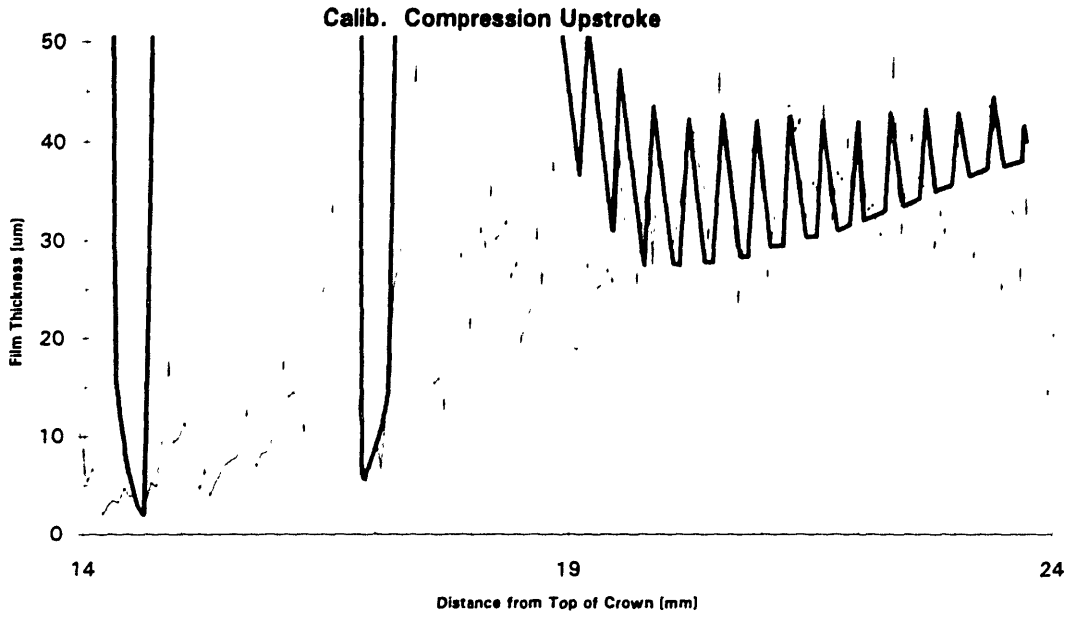


Figure 6.5 LIF calibration graph showing OC rail fit along with skirt machining mark match.

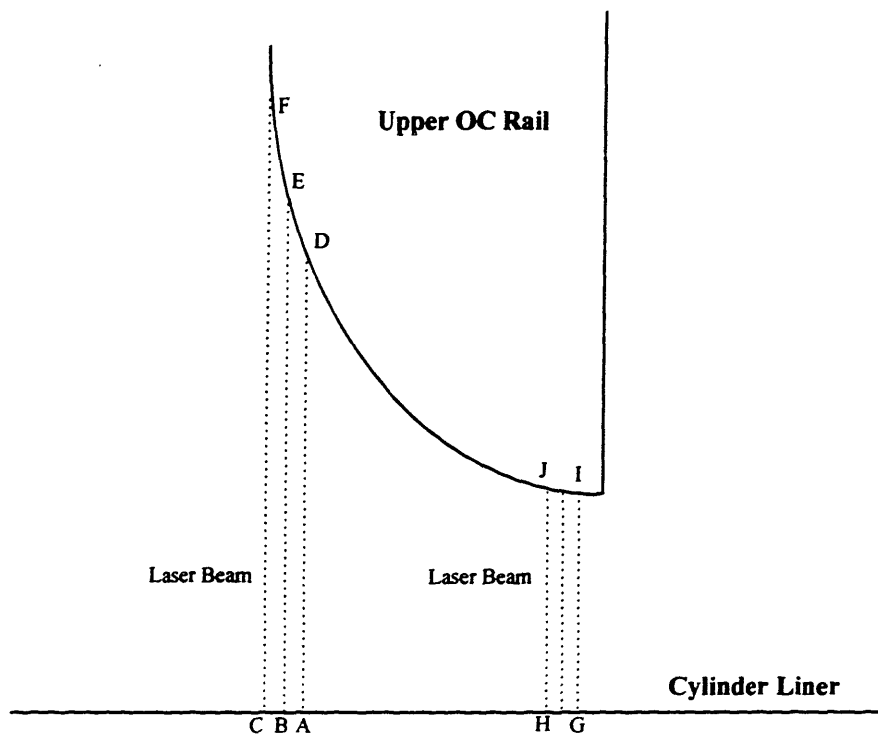


Figure 6.6 Laser beam impinging on OC rail at different wedge locations.

the error introduced by an over-flooded OC rail. Distance BE is the oil film thickness that we wish to record. However, since the laser beam has a finite width AC, the volume of oil sampled by the laser is ACFD. Since the LIF calibration is done on low constant slope regions such as GHJI on the OC rail or on the piston skirt, the ACFD oil volume ends up representing a film thickness greater than the actual thickness BE. What this results in is an oil trace which shows an OC rail valley narrower than the actual rail width. A graph of a lower OC rail which does not fit into its LIF trace because of excessive oil flooding is shown in Figure 6.7. A graph of the same OC rail which does fit into its LIF trace because there was not as much oil flooding is shown in Figure 6.8.

An interesting observation was that, on many data sets, the upper OC rail's upper face seemed to be flooded with oil even on the downstroke. A possible mechanism which would result in this is that on the downstroke, the second ring scrapes down whatever oil was in front of it, and that fluid circulates up to and around the third land region and ends up at the face of the upper OC rail. Since we are not certain of this mechanism, the calibration was never performed using the downstroke upper OC rail trace.

#### **6.4.3 LIF Calibration for Top Center Window**

For the Kohler engine used in this experiment, the top center LIF window was rendered useless by combustion and burnt oil residue build-up. The laser transmission through the sludge on the window was so bad that in order to obtain a readable voltage amplitude, the PMT voltage had to be cranked up to the point where the LIF oil film detail was destroyed by the PMT noise.

In addition, we hoped to calibrate the top center window LIF signal by using the crown land tool marks (similar to the upper-skirt tool marks). However, for fired conditions, the crown land in this engine runs dry, i.e. the film thickness on the crown land is the same as that on the free-liner ( $h_{\infty}$ ) with no signs of crown land tool marks. To make matters worse, even if the crown land were to run wet, there is so much combustion residue on it that the tool marks can not possibly appear on the LIF trace. Thus, acquiring fired LIF data from the top center window was ruled out.

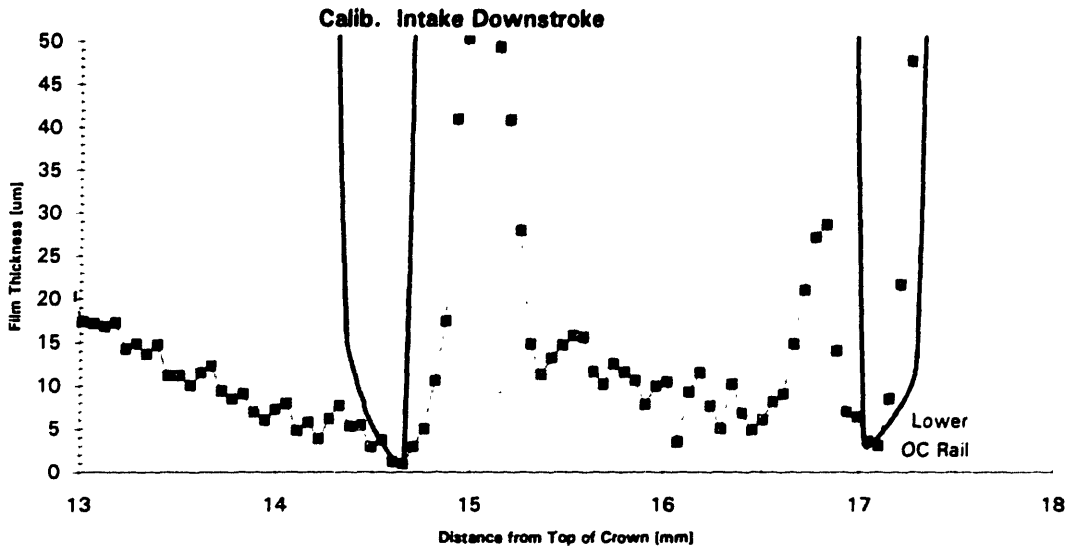


**Figure 6.7** Illustration of how an over-flooded lower OC rail results in an LIF trace too narrow for the OC rail Talysurf profile.

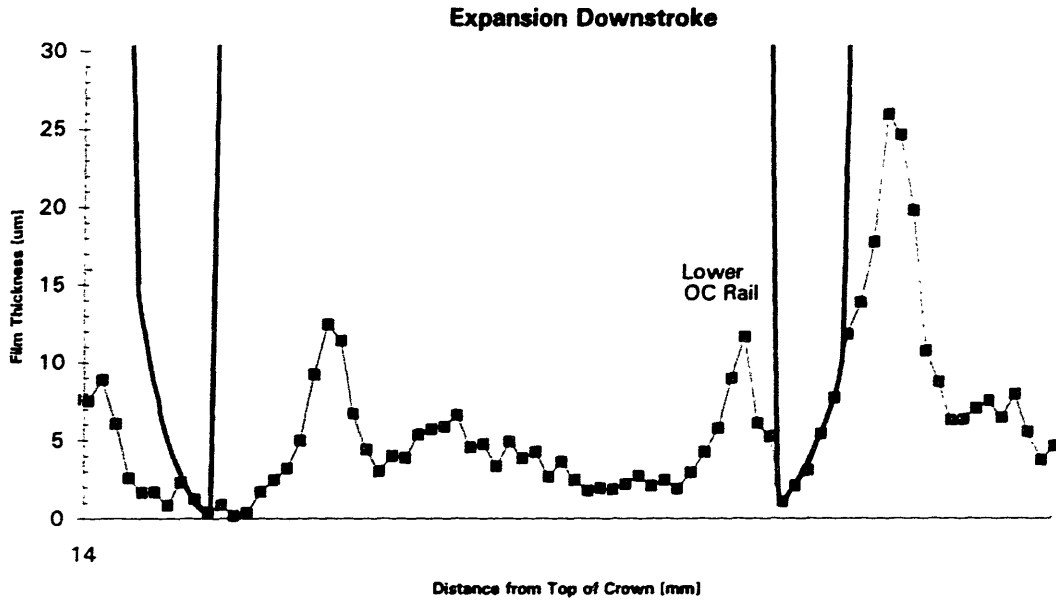


**Figure 6.8** Good lower OC rail fit.

Another problem with trying to use the crown land tool marks is that the crown land region wore significantly over the course of the experiments, probably due to piston slap. Therefore, the Talysurf profiles of the crown land tool marks taken before the experiments can not be used to calibrate a data set taken halfway through the test matrix. An alternate top center window calibration method may be to use a midstroke calibration coefficient multiplied by the relative laser transmission efficiency ratio of the two windows (Section 6.4.1).

#### 6.4.4 LIF Calibration vs. Liner Temperature and Oil Grade

The temperature and viscosity of the lubricant can have an effect on the calibration constant of the LIF signal. Bench experiments have been conducted by other LIF users [16] to determine the viscosity and temperature trends for the LIF signal. However, this would require that the probe focus, LIF window light transmissibility, fiber-optic cable transmissibility, and laser and PMT power to remain consistent throughout the entire test matrix.

For the particular engine used for the experiments, the window light transmissibility among the windows varied by over 20%, as measured by a hand-held laser power meter. Also, specific fiber optic cables had to be used for some of the windows for probe accessibility, and the transmissibility of those cables varied by as much as 30%. To make matters worse, due to the harsh vibration of a single-cylinder engine, the LIF focusing probe occasional came loose and out of adjustment. For these reasons, bench tests were ruled out. Without the bench test constraints, we were able to set the PMT voltage at the optimum level for each running temperature, thus maximizing the signal-to-noise ratio for each data set. A table of PMT voltage vs. cylinder liner temperature is given in Table 6.1. The PMT voltage for the 100 deg. C case could have been increased slightly up to 700 volts, but it was kept at 680 volts as a safety measure to keep the signal-to-noise ratio acceptable (Figure 2.2).

Cylinder Liner Temp. [deg.C]	PMT Voltage [volts]
40	580
60	650

80	680
100	680

**Table 6.1** PMT voltage for various liner temperatures.

### 6.5 ACCURACY TOLERANCE OF LIF OIL FILM THICKNESS

The accuracy analysis of the LIF oil film thickness is based on the accuracy of the calibration method(s). For the piston upper-skirt machining mark calibration method, the worse case scenario is for a maximum piston tilt of 0.5 degrees [17], (does not apply to windows located on wrist pin axis.) combined with a piston tilt of 0.5 degrees with respect to the Talysurf table. The reason for the latter tilt is due to the piston's barrel-shaped skirt which made squaring and clamping the piston to the Talysurf table somewhat difficult. The piston skirt machining marks have a slope of approximately 6 degrees, so the worse case error is 1 degree out of the target 6 degrees, or a +/- 16.6 % worse case error. Alternatively, the accuracy tolerance can be found by referencing the amplitude of the skirt teeth for the same result.

A similar accuracy analysis can be performed for the OC rail calibration method. The slope of the OC rail face is about 3.7 degrees. Unlike for the piston, squaring up and clamping the OC rail to the Talysurf table was not a problem. Therefore the worse-case total uncertainty of reading the 3.7 degrees of OC rail slope is due to the 0.5 degrees of piston tilt. The resulting LIF accuracy tolerance from the OC rail calibration method is  $0.5/3.7$  or +/- 13.4 %.

Since both methods are employed for all the LIF sets, it is safe to say that the worse case LIF oil film thickness accuracy is +/- 16.6 %. Though this figure may seem frightening at first, it is actually comforting to know that for a measured oil film thickness of 2 microns, the maximum error is only 0.3 microns.

The last questionable aspect of the OC rail calibration method is the tilt or twist of the ring within the ring groove. This is discussed in further detail in Section 10.1.

## CHAPTER 7 THEORY

### 7.1 PISTON RING LUBRICATION THEORY

The main purpose of the engine lubricant is to separate the metal rubbing surfaces to reduce friction and wear. The focus of this study is to investigate how the oil gets in between the piston rings and the cylinder liner. Figure 7.1 shows a schematic of a piston ring, the liner and a definition of the coordinate system. The origin of the  $X$ -axis is defined as the lowest point of the ring denoted  $x_0$ . The location where the oil begins to wet the ring is defined as  $x_1$ , and where the oil separates from the ring is defined as  $x_2$ . The location where the subring pressure peaks is defined as  $x_3$ . Notice that we have chosen a convention in which the liner moves relative to the ring with velocity  $U$ .

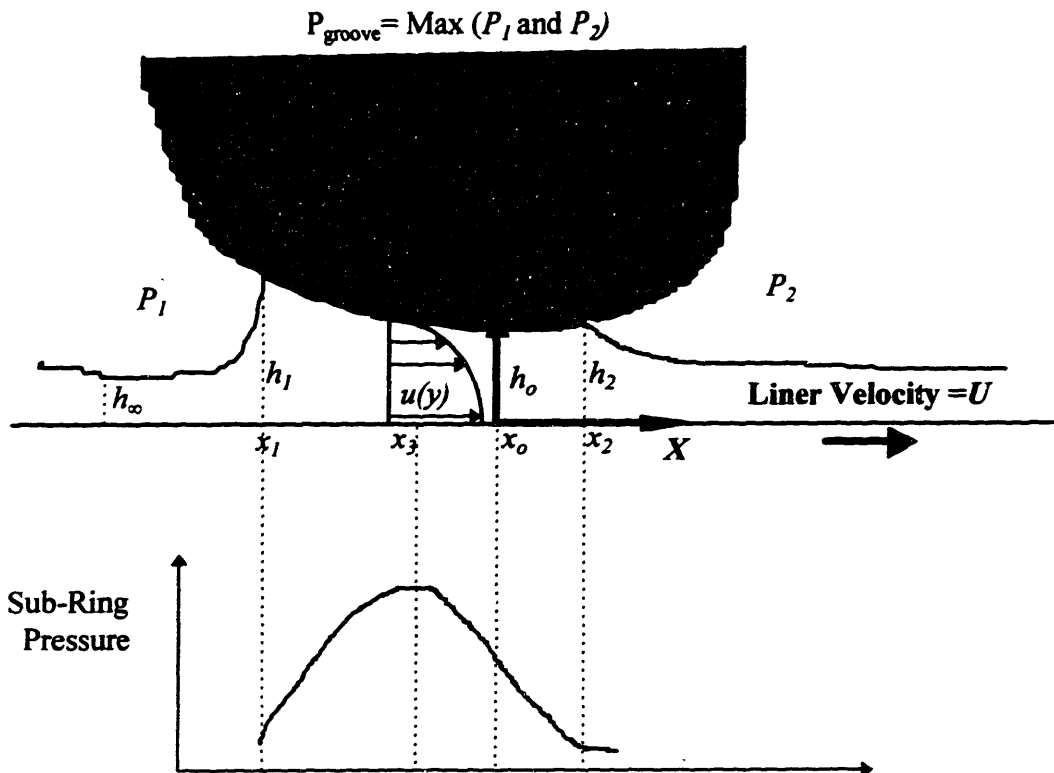


**Figure 7.1** Schematic of ring and liner and its coordinate system definition. Plot below shows pressure distribution under ring which produces lift.

The mechanisms by which the rings are “lifted” from the liner surface are discussed in the following sections.

### 7.1.1 Oil Film Thickness Calculation

To calculate the oil film thickness under the piston rings, we can start with the Navier-Stokes equation for steady-state parallel laminar flow,

$$\mu \frac{\partial^2 u(y)}{\partial y^2} = \frac{\partial P}{\partial x}, \quad (7.1)$$

where  $\mu$  is the fluid dynamic viscosity and  $P$  is the fluid pressure. Equation 7.1 can be integrated twice with respect to  $y$  to solve for the velocity profile  $U(y)$  using the boundary conditions: at  $y = 0$ ,  $u(y) = U$ , and at  $y = h$ ,  $u(y) = 0$ . The velocity profile can be written,

$$u(y) = \frac{1}{2\mu} \frac{\partial P}{\partial x} y(y - h) + U\left(1 - \frac{y}{h}\right). \quad (7.2)$$

The first term on the right hand side of Equation 7.2 represents the parabolic Pousueille flow, and the second term represents the linear Couette flow. The two flows combined results in a flow field which looks similar to the  $u(y)$  profile shown in Figure 7.1.

Once we have solved for the fluid velocity profile, we must next solve for the relationship between the pressure ( $dP/dx$ ) and the film thickness ( $h(x)$ ). Combining the continuity equation of the flow shown in Figure 7.1 with Equation 7.2, we can write for any  $x$  under the ring,

$$Uh_{\infty} = \left[ \int_0^h u(y) dy \right] + (\text{unsteady.terms}) = \left[ -\frac{h^3}{12\mu} \frac{dp}{dx} + \frac{Uh}{2} \right] + (\text{unsteady.terms}). \quad (7.3)$$

For the midstroke region, the unsteady terms in Equation 7.3 are negligible. In this case, we can rearrange Equation 7.3 to obtain,

$$\frac{dP}{dx} = \frac{6\mu U}{h(x)^3} (h(x) - 2h_{\infty}). \quad (7.4)$$

This is a steady state integral form of the Reynold's Equation [18].

The three unknowns of the oil film thickness under the ring are: the entrance location  $x_1$ , the exit location  $x_2$ , and the minimum oil film thickness (MOFT)  $h_0$ . Therefore, we need three equations to solve for the three unknowns. The first equation is Equation 7.4 integrated with respect to  $x$  from  $x_1$  to  $x_2$ ,

$$P_2 - P_1 = \int_{x_1}^{x_2} \frac{6\mu U}{h(x)^3} (h(x) - 2h_{\infty}) dx. \quad (7.5)$$

The second equation is a force balance between the ring tension and the hydrodynamic lift [19] which can be expressed as,

$$\int_{x_1}^{x_2} P(x) dx + (x_1 + B_1)P_1 + (B_2 - x_2)P_2 = L + (B_1 + B_2)(P_{groove}), \quad (7.6)$$

where,  $L$  represents the elastic ring tension load,  $P_1$  and  $P_2$  represent the land pressures in front of and back of the ring, respectively, and  $B_1$  and  $B_2$  represent the half-widths of the piston ring (Figure 7.1). The land pressures are obtained from a piston gas dynamics program such as GASFLOW.

To arrive at a third equation, we must make an assumption about the exit condition that at the trailing edge of the ring ( $x=x_2$ ) [20],

$$\left. \frac{dP}{dx} \right|_{exit} = 0. \quad (7.7)$$

Equation 7.7 is known as the Reynolds exit condition. The three nonlinear algebraic equations (Equations 7.4, 7.5, and 7.6), can be solved simultaneously by an iterative method such as Newton's Method.

To incorporate the shear-thinning effect of a non-Newtonian oil, the viscosity  $\mu$  must be made a function of the shear rate  $dU/dy$ , in which case a two-step iteration must be performed. Equation 7.1 can not be directly integrated into Equation 7.2, since viscosity and shear rate both have to be solved iteratively. The shear-thinning effect, most prominent in multi-grade oils, is discussed in Section 3.2.

As the piston velocity approaches zero, the unsteady terms in Equation 7.3 become important; that is, the velocity of the ring face as it moves away from the liner ( $dh_o/dt$ ), and the rate in which the location where the oil starts to wet the ring changes ( $dx_1/dt$ ) become non-negligible. For the unsteady case, Equation 7.3 can be rewritten [23],

$$Uh_\infty = \left[ -\frac{h^3}{12\mu} \frac{dp}{dx} + \frac{Uh}{2} \right] + (x - x_1) \frac{dh}{dt} - (h_1 - h_\infty) \frac{dx_1}{dt}. \quad (7.8)$$

### 7.1.2 Wedge Effect

The most dominant mechanism in piston ring lubrication is hydrodynamic lift created by a wedged surface. Notice from Equation 7.3 that for a constant volume flow under steady-state conditions (liner velocity  $U$  is constant), a spatially varying  $h$  such as that found under a ring wedge will result in the non-constant  $dp/dx$  necessary to produce ring lift. The sub-ring film thickness and pressure profile necessary to produce ring lift, as depicted in Figure 7.1, can be constructed from Equation 7.4. From the assumption that  $dp/dx = 0$  at the exit, we see that  $h|_{x_2} = h_2 = 2h_\infty$ . We know that for ring lift to be produced, the pressure gradient from  $x_1$  to  $x_3$  must be positive ( $dp/dx > 0$ ). From Equation 7.4, we see that in  $x_1$  to  $x_3$  region, the subring film thickness is greater than  $2h_\infty$ . The subring pressure reaches its peak at some point  $x_3$ , where  $dp/dx = 0$ , and  $h_{x_3} = 2h_\infty$ . Then, in the region of  $x_3$  to  $x_2$ , the film thickness is less than  $2h_\infty$ ,

i.e.,  $dp/dx$  is negative (downward slope as shown in lower graph of Figure 7.1). It is this subring pressure profile which pushes the ring up off the liner surface in the presence of a wedge surface.

### **7.1.3 Corner Effect**

When an asymmetric piston ring such as the upper OC rail shown in Figure 5.6 moves across the piston liner, it must produce lift on both the up and downstrokes. The upper OC rail, on its upstroke, produces lift by the wedge effect described in Section 7.1.1. However, on the downstroke, the leading face of the upper OC rail is very abrupt and can not be modeled as a wedge. The lift then must be produced by another mechanism, the “corner effect.”

The corner effect assumes that the fluid flowing toward the steep side wall of the upper OC rail initially produces no lift, and the ring slides across the liner under boundary lubrication conditions. The fluid runs into the steep side wall and is forced to flow up the side wall. The stream line solution of this type of flow field [21] results in an infinite pressure point at the corner where the tip of the OC rail meets the liner. However, in actuality, there are many surface asperities on the OC rail and liner which give rise to gaps between the OC rail and the liner. Since the fluid in these asperities are exposed to the high pressure generated at the rail-to-liner corner, OC rail lift is generated. Once the fluid gets past the corner region, the pressure distribution under the wedge region of the OC rail can be calculated in the same way it was for the wedge effect.

### **7.1.4 Squeeze Effect**

An important result of the unsteady case mentioned in Section 7.1.1 is that even at the endstrokes where the piston velocity is zero, there can still be fluid flow under the rings. Notice that in Equation 7.8, even for a liner speed  $U = 0$ , a pressure profile similar to that shown in Figure 7.1 can be generated under the ring. Depending on the sign of the sub-ring pressure profile slope ( $dp/dx$ ), the flow can be in the positive or negative  $X$ -direction. In other words, the squeeze

**effect results in the fluid squeezing out from under the rings from both sides as the MOFT decreases as the piston approaches the endstrokes.**

## CHAPTER 8 EXPERIMENTAL RESULTS AND ANALYSIS

The following sections describe the LIF results of the multi-windowed Kohler engine. Since it is impossible to summarize all the results in a single graph format, a variety of graphs have been constructed, each designed to emphasize one or more trends. Some of the trends discussed in the following sections are intentionally qualitative in nature. The reasons for this are:

- 1) It is difficult to determine the actual viscosity of the oil under engine running conditions (Section 3.2).
- 2) It is difficult to assess the actual bore distortion because the engine was measured cold (Section 5.1).

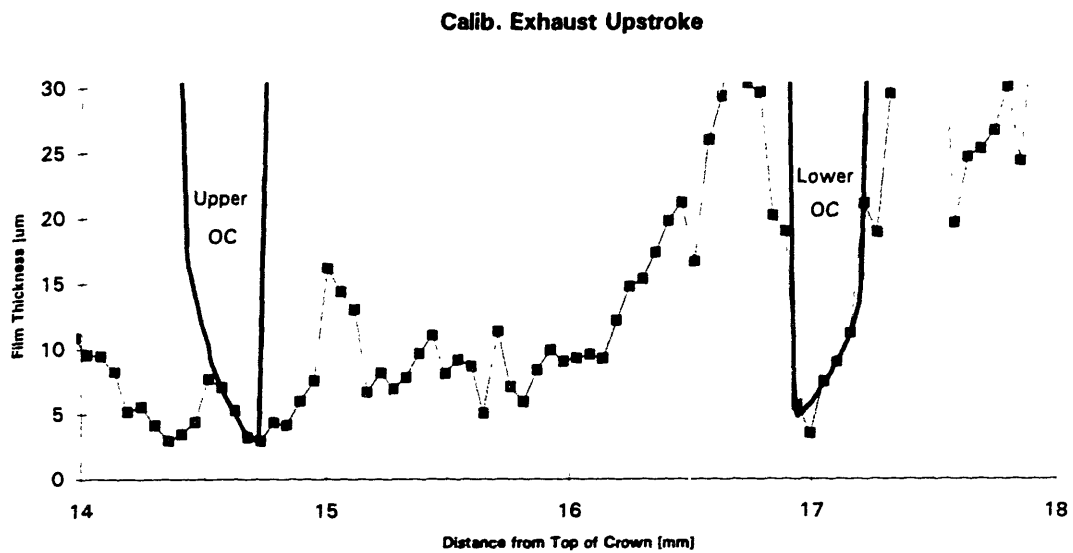


**Figure 8.1** Example of the improved resolution OC rail trace.

### 8.1 RELATIVE FILM THICKNESSES AMONG THE FREE-LINER, THE TOP TWO RINGS AND THE OIL CONTROL RAILS

The free-liner oil film thickness ( $h_{\infty}$ ) was obtained by averaging roughly 300 points on the liner (corresponds to about 12 mm along the liner) above the top land. Section 6.1 describes at which

portion of the engine cycle the  $h_{\infty}$  was recorded. The major importance of the  $h_{\infty}$  is its relation to the top ring. The  $h_{\infty}$  is the oil supply for the top ring on the upstroke, and what the top ring leaves behind on the downstroke for the following upstroke. Calculations predict that the MOFT under the top ring is slightly less than twice the free-liner film thickness  $h_{\infty}$ . This can easily be seen by matching the velocity profile areas at the free-liner (uniform velocity = rectangular velocity profile) to that at the MOFT (approximately triangular velocity profile). Then, since the top ring is not fully flooded, the second ring should have about the same MOFT as the top ring.

The OC rails come next. In previous experiments, we have never been able to get accurate OC rail MOFT readings because of signal aliasing. Now that the sampling frequency has been doubled, we can regularly trace the OC rail face contour with four or more data points. An LIF trace of the OC rails is shown in Figure 8.1. This trace is a single-cycle trace, and the upper OC rail (left rail) wedge was used to calibrate the signal.

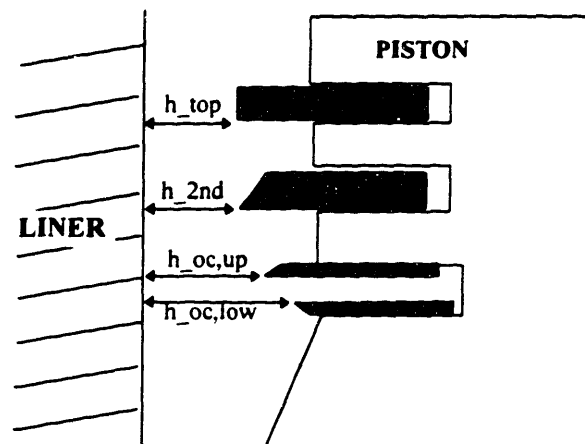


**Figure 8.2:** Schematic of the hierarchy of the MOFT's under the piston rings for both the downstrokes and the upstrokes.

For practically every data set, the experimental data shows that both OC rails have thicker MOFT's than the top two rings, and the lower OC rail always has a thicker MOFT than the upper OC rail. This "hierarchy" of film thicknesses within the ring pack is shown schematically in Figure 8.2. What is particularly interesting is that this hierarchy holds for both the downstrokes and the upstrokes.

The experimental results for the mono-grade 10W oil during a downstroke is shown in Figure 8.3. Notice in Figure 8.3 that for each liner location (windows 1,2,4,6), the film thickness hierarchy is as shown in Figure 8.2. The bottom center window (window #6) does not see a free-liner film thickness because the piston never travels low enough relative to that window. What is also noticeable from Figure 8.3, is the difference between the MOFT at midstroke and bottom center. The MOFT at window #1 (midstroke) is greater than that at window #6 for all the rings. It is not valid to compare the film thicknesses from the other two midstroke windows (windows #2 and #4) to the bottom center window because of the bore distortion effect described in Section. 5.1. Additional graphs for the other strokes are shown in Figures D.1 ~ D.3 in Appendix D.

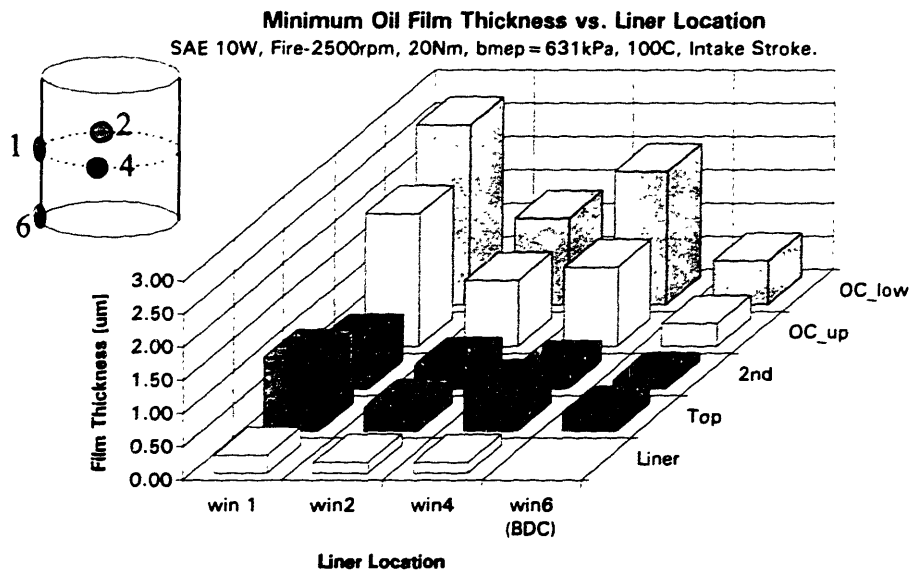


**Figure 8.3** MOFT vs. liner location. Shows trends of: windows (circumferential, axial), rings, speed (mid vs. BDC) for SAE 10w oil. Data has been averaged over ten cycles.

As discussed in Section 2.2.1, the lower OC rail experiences the smallest velocity change as it travels from the midstroke window (window #1) to the bottom center window (window #6). Therefore, we expected the percentage change between the OC rail MOFT at midstroke and that at bottom center to be the least for the lower OC rail. However, as Figure 8.3 shows, this percentage difference is approximately the same as that for the top ring. It was thought that a possible explanation may be that the squeeze term (Equation 7.7) of the OC rail is much less

than that for the top two rings, so a small decrease in ring velocity results in a large decrease in film thickness. However, this probably is not the case since the OC rail film thickness did not change drastically from 2500 rpm to 1800 rpm.

The hierarchy of the MOFT under the rings, shown schematically in Figure 8.2, for both downstroke and upstroke can be qualitatively explained by the following scenario. We shall first start with the downstroke. In the previous upstroke, the piston skirt has just brought a fresh supply of oil to the cylinder liner. As the piston progresses down:

- 1) The lower OC rail encounters a large mass of oil and develops lift by the wedge effect. Since there is a large oil supply, there is a large wetted width under the ring and substantial lift is produced.
- 2) The upper OC rail encounters the oil left by the lower OC rail and whatever oil was accumulated between the rails. The rail lift is produced by the corner effect. Due to the lack of a wedge and a smaller oil supply, the upper OC rail develops less lift than the lower OC rail. The result is a larger MOFT for the lower OC rail over the upper OC rail.
- 3) The second ring encounters the oil left by the upper OC rail and whatever oil that was accumulated in the third land and re-deposited on the liner. The second ring fully floods and scrapes oil down the liner and accumulates oil in the third land. By mass conservation, the second ring results in having a smaller MOFT than the upper OC rail. Another way of thinking about this is if the second ring did not scrape down any oil, the MOFT of the second ring and the upper OC rail should be the same.
- 4) The top ring is not fully flooded, so whatever passes under the second ring, passes under the top ring. This results in the top ring having about the same MOFT as the second ring, as we have seen in most of the data.

On the following upstroke,

- 1) The top ring encounters the  $h_{\infty}$  that it left behind on the previous downstroke. The top ring does not fully flood, so whatever the top ring encounters passes under it.
- 2) The second ring encounters the oil left by the top ring. The second ring does not perform any scraping duties since it does not fully flood as it does on the downstroke. Since the oil volume passing under the top ring and second ring are the same, the MOFT of the second ring should be the same as that of the top ring.

3) The upper OC rail encounters the oil left by the second ring and the oil accumulated in the third land from step (3) of the downstroke. Due to the extra oil supply and the more aggressive wedge profile of the upper OC rail (3.7 degree slope vs. 0.65 degrees for the second ring), the upper OC rail develops greater hydrodynamic lift than the second ring, resulting in a greater MOFT.

4) Finally, the lower OC rail encounters the oil left by the upper OC rail and the abundant oil supply accumulated in the OC expander spring. It is possible that this great oil supply and the corner effect results in enough lift to make the MOFT of the lower rail greater than that of the upper rail as shown in the data. Another phenomena which may play a role is the tilt of the OC rail with respect to the piston groove. The tilt however is probably not very significant because the LIF plots are scaled with microns on the vertical axis and millimeters on the horizontal axis. A very minute tilt will show up as a great exaggeration in the ring profile, and would lead to tremendous ring profile-to-LIF trace misfits.

Figures 8.4 and 8.5 show the same type of plot as Figure 8.3, except the oil used was a multi-grade 10w50 and a mono-grade SAE 50 oil, respectively. Notice that aside from the absolute value of the film thickness, and the occasional irregularity in the lower OC rail film thicknesses, the relative ring trends are consistent for all three oils.

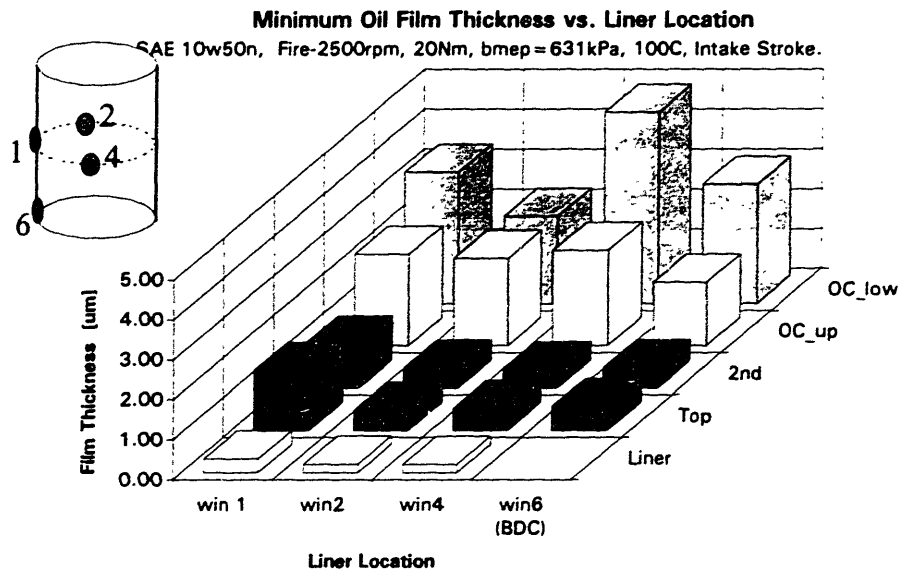


**Figure 8.4** MOFT vs. liner location. Shows trends of: windows (circumferential, axial), rings, speed (mid vs. BDC) for 10w50 oil. Data has been averaged over ten cycles.

Regardless of whether the film thickness variation among the rings can be explained, it is important to realize that the Kohler ring pack is performing its task superbly. On the downstroke, the role of the ring pack is to seal the combustion chamber (top ring and second ring) and to scrape oil off the liner to control oil consumption. In order to seal the combustion chamber, the MOFT of the top two rings must be relatively smaller than those of the OC rails. And in order to scrape the oil off the liner, the MOFT's under the rings must get progressively thinner, from the lower OC rail up to the second ring, as the rings scrape more and more oil off the liner.

On the upstroke, the top two rings must still seal the combustion chamber, and the OC rails must carry fresh oil up the liner. Again, to perform this task, the top two rings must have relatively lower MOFT's, and the MOFT's should get progressively greater, from the second ring down to the OC rails, to bring as much oil to the liner while still controlling oil consumption. Another reason for this film thickness hierarchy is to prevent excessive oil accumulation in the piston lands and piston grooves from the previous downstroke.

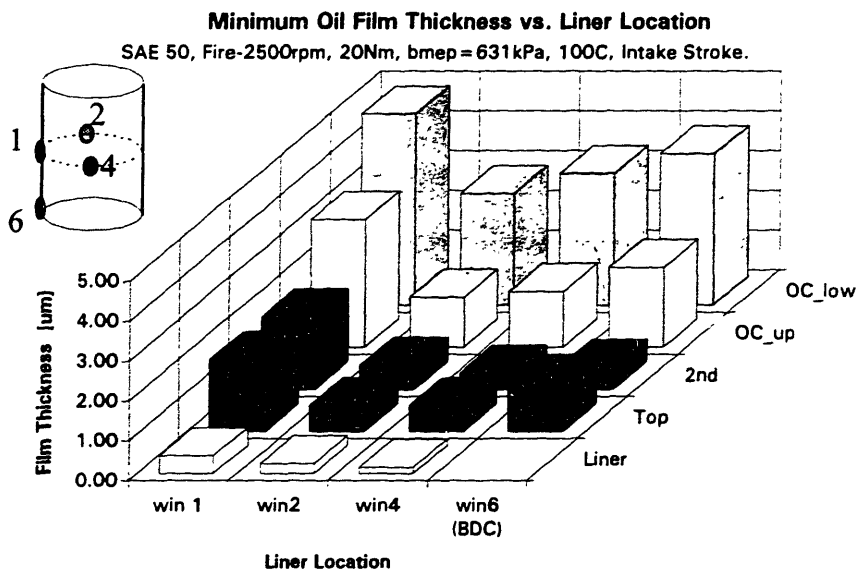


**Figure 8.5** MOFT vs. liner location. Shows trends of: windows (circumferential, axial), rings, speed (mid vs. BDC) for SAE 50 oil. Data has been averaged over ten cycles.

## 8.2 LINER LOCATION TREND

The circumferential variation in film thickness may be caused by a variety of geometric and dynamic effects. The most dominant cause of circumferential oil film thickness variation is probably the cylinder liner bore out-of-roundness. The bore distortion plot measured after the experiment is shown in Figure 5.1. The thrust side (12 o'clock position) shows noticeable wear relative to the regions of the liner along the wrist pin axis (windows #2 and #4). Though this bore measurement was made with a cold engine, we can assume that for a piston assembly with axisymmetric ring tension distribution, the excessive thrust side wear will contribute to a circumferential film thickness variation.

There are two schools of thought on how bore distortion caused by liner wear affects film thickness. One thought is that since the thrust side is so worn, the ring can not conform into the wear valley and the effective ring tension on that portion of the liner is reduced. This would result in a thicker film thickness on the worn thrust side (window #1) relative to the rest of the liner under steady state conditions. Since the wear at the windows #2 and #4 look similar, we expect the film thickness at those windows to be comparable. Perhaps the rings only fully seat into the wear valley under heavy acceleration or during piston slap. The second school of thought is that the ring conformability is actually better in the wear valley because it was the rings scraping against the liner that wore it out in the first place. The liner will continue to wear until the rings conform perfectly to the liner. In this case, the film thickness at the thrust side window would be equal or less than those at windows #2 and #4 due to equal or greater local ring tension, respectively. Another geometric variable that may influence the film thickness is the total lack of a piston skirt at the window #4 location along the wrist pin axis.

The liner location trend can best be summarized by Figure 8.6. This graph shows the MOFT of the top ring for all three oils as seen from the four LIF windows. The liner location trend shown in Figure 8.6 is the former of the two schools of thought described above. The MOFT's at windows #2 and #4 are comparable, but the MOFT at window #1 is greater than both of them by about a factor of two. Also, the MOFT's at window #1 (midstroke, thrust side) are greater than those at window #6 (bottom center, thrust side) by about a factor of 1.5.

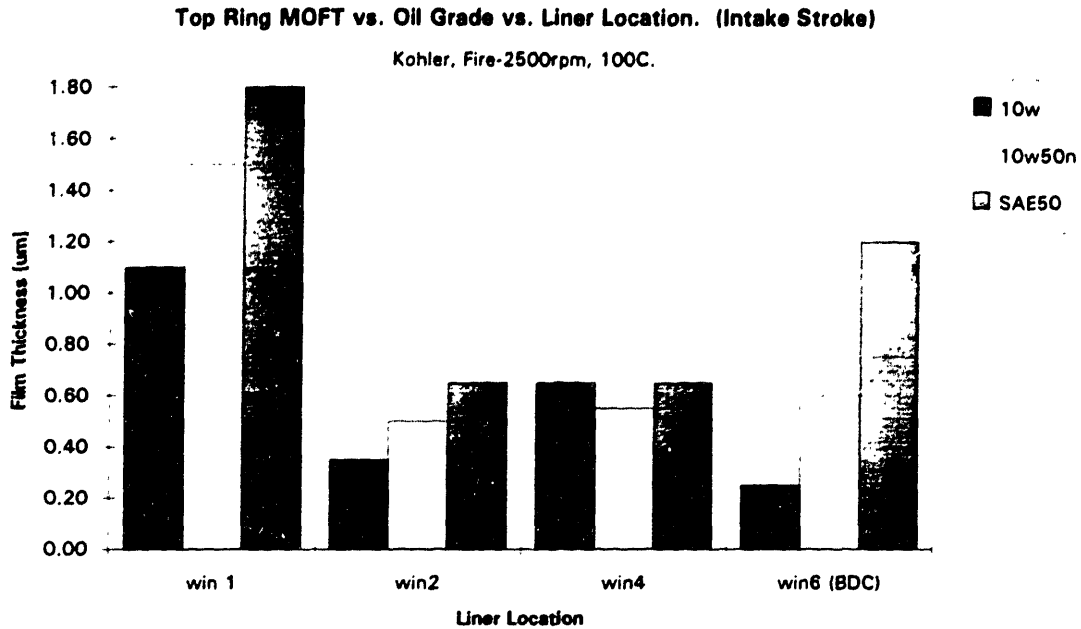


**Figure 8.6** Top ring MOFT vs. oil grade vs. liner location. Shows trend of: windows, skirt, and oil viscosity. Clearly illustrates viscosity trend for each window. Data has been averaged over ten cycles.

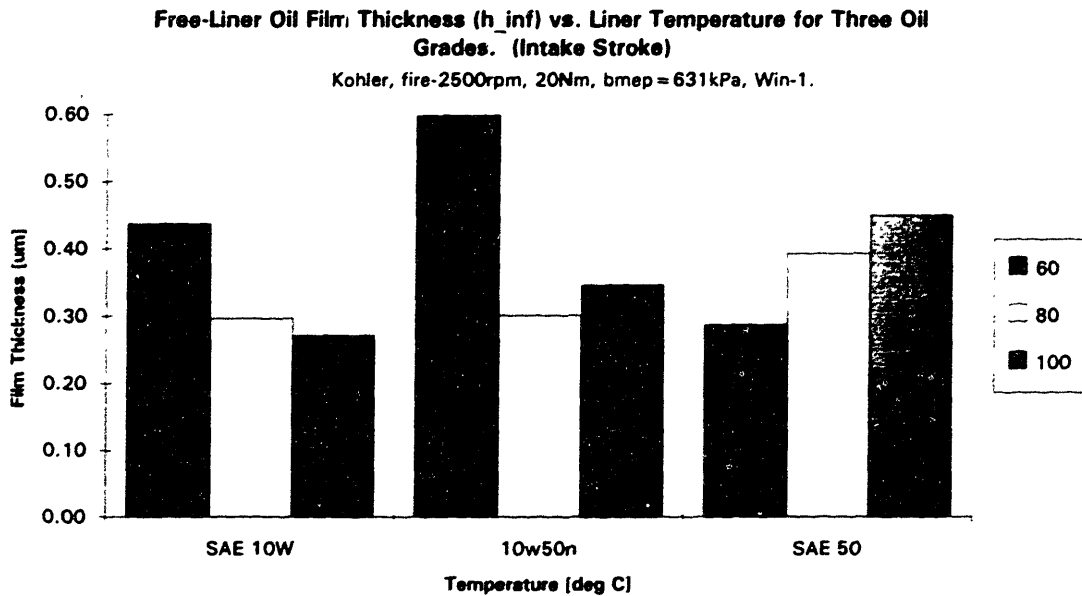


**Figure 8.7** Free-liner film thickness vs. liner temperature vs. oil grade. Shows trend of: liner temperature, oil viscosity, shear-thinning effect. Notice that low temperature SAE 50 oil's film thickness is relatively small. The trends generally hold for the top two rings also. Data has been averaged over ten cycles.

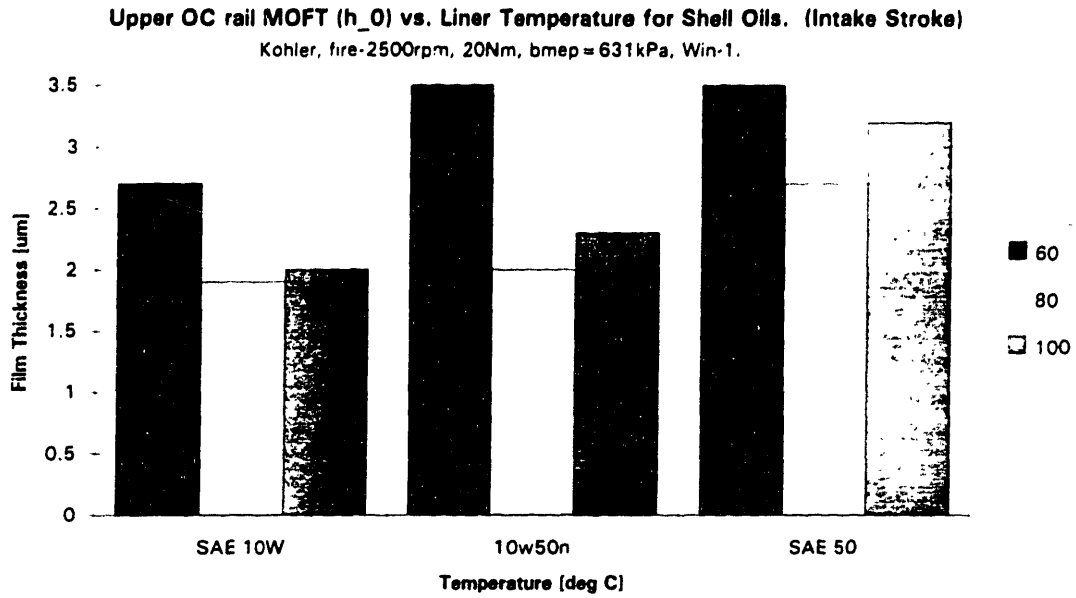


**Figure 8.8** Upper OC rail MOFT vs. liner temperature vs. oil grade. Shows trends of : liner temperature, oil viscosity, shear-thinning effect. For OC rails, the low temperature SAE 50 oil's film thickness is not relatively small, as in Figure 8.6. Data has been averaged over ten cycles.

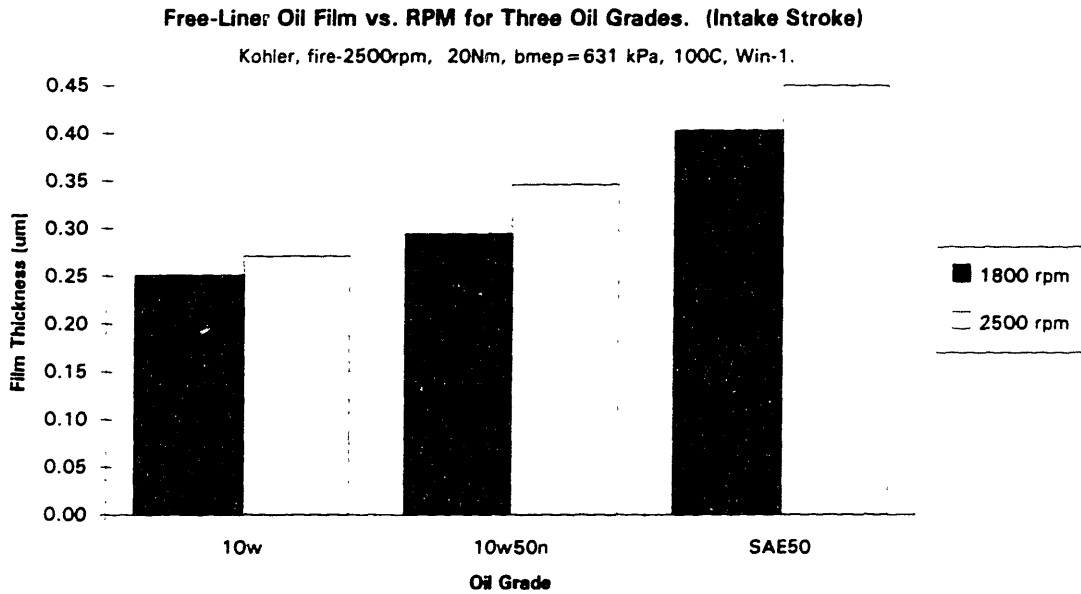


**Figure 8.9** Free-liner film thickness vs. engine speed vs. oil grade. Shows trend of: engine rpm, oil viscosity, and shear-thinning. Data has been averaged over ten cycles.

### 8.3 OIL VISCOSITY AND TEMPERATURE TRENDS

Calculations show that the MOFT is roughly proportional to  $\sqrt{\mu}$ . This upward trend is expected since as oil viscosity increases, the pressure generated under the ring can increase and result in greater oil film thickness. Since the thickest oil (SAE 50) used in the experiment has a viscosity some 300 % greater than the thinnest oil (SAE 10W), we expected to be able to detect noticeable film thickness differences. However, for extremely high oil viscosities, it is possible that an oil pumping problem may occur which can deplete the liner of a sufficient oil supply. This phenomenon is probably very engine specific and would be difficult to model without extensive knowledge of the entire engine lubrication system.

The film thickness to oil viscosity trend has already been shown in Figures 8.3 through 8.6. For all the rings and the free liner, as the oil viscosity increases, so does the oil film thickness. For example, as shown in Figure 8.6, there was about a 65% increase in the top ring MOFT when the oil grade was switched from SAE 10W to SAE 50.

Figure 8.6 also shows the oil viscosity trend very clearly. For example for window #1, as the viscosity grade increases from SAE 10W up to SAE 50, the MOFT also increases. This clear upward trend can also be seen at window #2 as well as at the bottom center window #6. However, there does not seem to be any viscosity trend at window #4. The reason for this can not be completely explained but probably has to do with the fact that window #4 is located at a circumferential location where the piston does not have a skirt segment at all (oil drain groove location). Perhaps the absence of a skirt disturbs the oil supply mechanism to this region of the ring pack. The trends shown in Figure 8.6 (top ring, intake stroke) are representative of the other strokes and rings. Additional graphs are shown in Figures D.4 and D.5 in Appendix D.

The effect of temperature on oil film thickness is essentially a viscosity effect. As shown in Figure 3.1, oil temperature can have a dramatic effect on its viscosity. The calculations that would be performed for solving for the oil film thickness dependence on temperature is the same as that done for the viscosity dependence. Since the viscosity drops more steeply at lower temperatures, we can expect a greater film thickness difference between 60 and 80 deg. C, than

between 80 and 100 deg. C. More rigorous analyses can be performed which include the thermal expansion and deformation effects on engine components.

Figure 8.7 shows the effect of oil viscosity and liner temperature on the free-liner film thickness ( $h_{\infty}$ ). The temperature trend shown for the SAE 10w is the most obvious. As the liner temperature increases, the viscosity of the oil on the liner decreases, and the resulting film thickness is lower. A temperature increase from 60 to 80 deg. C decreases the oil viscosity by about 80 %, so the film thickness should decrease by about 35 %. The trends shown in Figures 8.7 and 8.8 for the SAE 10W and 10W50 oils show this trend within the accuracy tolerance of +/- 16.6 % described in Section 6.5. For example, for the free-liner, 10W50 oil case the measured film thickness at 60 deg. C is about 0.6 microns +/- 16.6 % (0.5 to 0.7 microns) and the measured film thickness at 80 deg. C is about 0.3 microns +/- 16.6 % (0.25 to 0.35 microns). A 35 % decrease in film thickness from the minimum allowable film thickness at 60 deg. C of 0.5 microns is 0.33 microns which is within the tolerance of the 80 deg. C film thickness.

As discussed earlier, the film thickness difference between the 80 and 100 deg. C cases should be less than that between the 60 and 80 deg. C cases. A temperature increase from 80 to 100 deg. C will lower the oil viscosity by about 40 %, so the film thickness should decrease by about 20 %. The trend for the multi-grade 10w50 oil is essentially the same as that for the SAE 10W case, except the 80 and 100 deg. C cases reversed order. However, this discrepancy is not a concern since it is within the +/- 16.6 % accuracy tolerance. However, the trend shown for the SAE 50 oil is surprising. The film thickness to temperature relationship is completely reversed - as the liner temperature increases, so does the film thickness. The cause of this may be the oil pumping difficulty of excessively high viscosity oils.

The temperature trends for the upper OC rail is shown in Figure 8.8. The trends for the SAE 10W and those for the 10w50 are comparable to the trends shown for the free-liner. However, the trends for the SAE 50 is again irregular.

The shear-thinning effect was also noticeable between the multi-grade 10w50 oil and the mono-grade SAE 50 oil. The two oils have similar low-shear viscosities, but quite different viscosities at high shear (Section 3.1). Since at high shear, the 10w50 oil shear-thins to about half its low-

shear viscosity, and the SAE 50 oil essentially maintains its low-shear viscosity. we expected the film thicknesses for the 10w50 oil to be about 30 % thinner than those for the SAE 50 oil. The shear-thinning effect can be seen in Figure 8.9. The experimental data shows about a 25 % decrease in film thickness as the multi-grade oil shear-thins from its low-shear to its high-shear viscosity. The discrepancy between the expected and experimental values is well within the +/- 16.6 % accuracy tolerance of the LIF system.

Due to the large amount of data, the motored data has not been processed at this time.

#### **8.4 ENGINE SPEED TREND**

The MOFT dependence on engine speed is shown in Figure 8.9. Note that for all three oils, the MOFT increases by 10 to 15 % for an engine speed increase from 1800 to 2500 rpm. The trends shown for the free-liner and intake stroke are very representative of the piston rings and the other engine strokes. The oil viscosity trend can also be clearly seen in this graph. For a given engine speed, as the oil viscosity grade increases from SAE 10W to SAE 50 at 100 deg. C, the free-liner film thickness increases some 75 %. Unfortunately, the 3500 rpm data sets were not usable due to faults in the data acquisition. As discussed in Section 2.3, the encoder should have been able to keep up with the engine, but data set looked as if the triggering of the data acquisition was completely random.

#### **8.5 OBSERVATIONS OF OIL MASSES ON PISTON LANDS AND SKIRT**

In addition to measuring oil film thicknesses under the rings and on the liner, the LIF system can also be used to gain insight into the behavior of oil masses accumulated in the piston lands and on the skirt. The MIT LIF system has been used in the past to measure the second land oil volume to study oil consumption [22]. One step beyond this is to study the dynamics of the oil masses as the piston reciprocates. For example, Figure 8.10(a) shows the upstroke and Figure 8.10(b) shows the downstroke, where the inertia of the oil in the third land skews the oil mass down (towards right of graph) on the upstroke, and up on the downstroke.

Another phenomenon that can be studied is which variables affect whether the crown land or second land run wet or dry. For example, the second land runs wet under the baseline running condition on the midstroke thrust side as shown in Figure 8.11(a), but runs wet about 90 degrees circumferentially around the liner from it as shown in Figure 8.11(b). Observations such as this are particularly important for oil consumption studies, since it has been assumed in the past that the second land oil film thickness was uniform around the circumference of the liner [4].

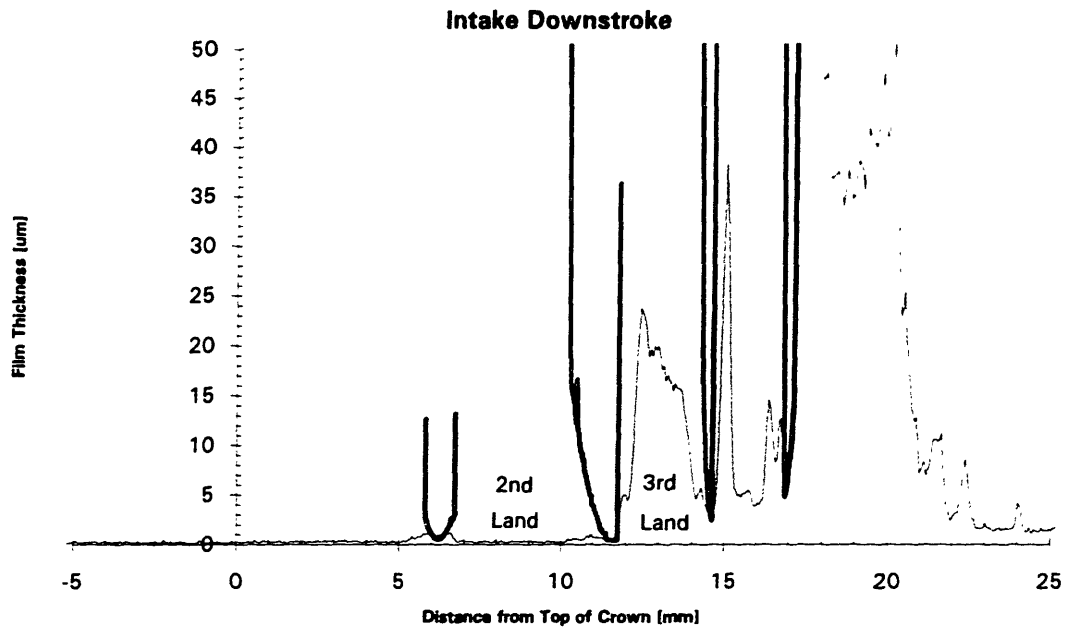


**Figure 8.10(a)** Third land oil volume skewed due to oil mass inertia. (Single trace, 10W50 oil, window #4, fire-2500 rpm, bmep=631 kPa.)

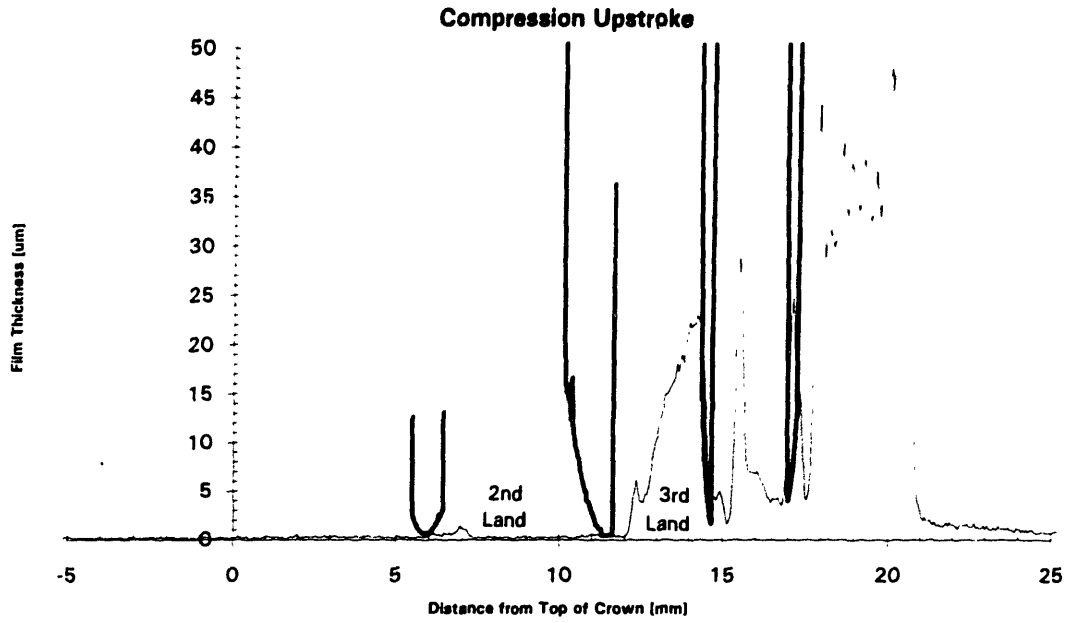


**Figure 8.10(b)** Third land oil volume skewed due to oil mass inertia. (Single trace, 10W50 oil, window #4, fire-2500 rpm, bmep=631 kPa.)

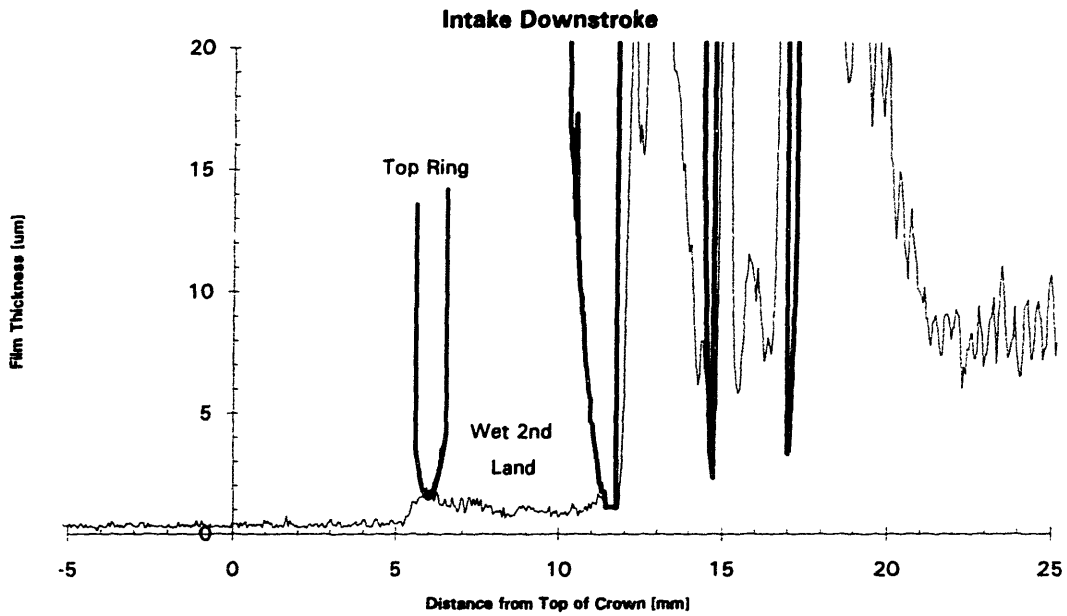


**Figure 8.11(a)** Wet second land for baseline running condition at window #1. (Single trace, 10W50 oil, window #1, fire-2500 rpm, bmep=631 kPa.)

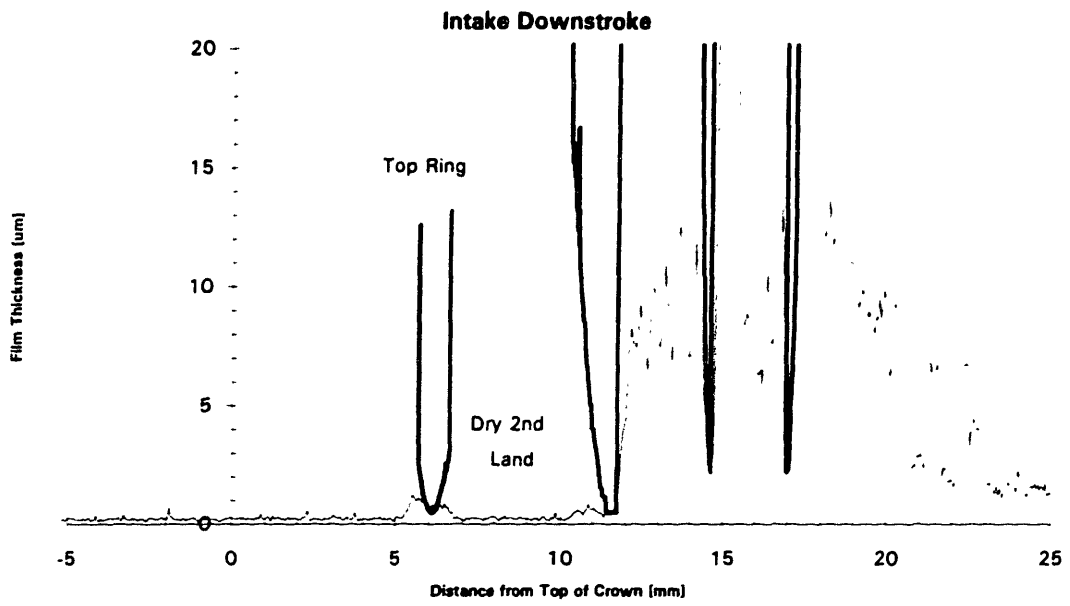


**Figure 8.11(b)** Dry second land for baseline running condition at window #2. (Single trace, 10W50 oil, window #2, fire-2500 rpm, bmep=631 kPa.)

## CHAPTER 9 CONCLUSIONS

- 1) The calibration method using the upper OC rail wedge profile was consistent with the piston skirt machining mark method. The calibration coefficient was typically about 75 mv/microns.
- 2) There were noticeable differences in film thickness among the four LIF windows. The circumferential film thickness data show that the bore distortion effects are significant. A radial bore distortion of 15 microns, measured in a cold engine block, resulted in film thickness differences among the windows of up to 300 %. The film thickness was greatest on the thrust side where the cylinder wear was most extensive. For example, the top ring minimum film thickness at midstroke for the baseline running condition (fired at 2500 rpm, 100 deg. C, bmep=631 kPa) with SAE 50 oil ranged from 0.7 microns to 1.8 microns (thrust side). The film thicknesses at midstroke (thrust side) was typically about a factor of 1.5 greater than those at bottom center on the thrust side.
- 3) The minimum oil film thickness under the rings increased with viscosity. The film thicknesses for the SAE 50 oil was about 65% greater than those for the SAE 10W oil. This roughly agrees with the expected  $\sqrt{\mu}$  trend for the approximately three-fold viscosity difference.
- 4) The shear-thinning effect is noticeable between the mono-grade SAE 50 and the multi-grade 10w50 oils. The experimental data shows about a 25% decrease in film thickness as the multi-grade oil shear-thins from its low-shear to its high-shear viscosity.
- 5) As the liner temperature increased, the film thickness decreased due to the drop in viscosity except for the SAE 50 case. The film thickness difference between the 80 and 100 deg. C cases was about 20 %, and that between the 60 and 80 deg. C cases was about 35 %. For the SAE 50 case, the film thickness to temperature relationship is completely reversed - as the liner temperature increases, so does the film thickness. The cause of this may be the oil pumping difficulty of excessively high viscosity oils.

6) The minimum oil film thickness under the piston rings increased with engine speed. The film thickness for the baseline engine speed of 2500 rpm was about 20 % greater than that for a speed of 1800 rpm.

7) Inertia of the oil mass in the piston lands is observable. For example, during the upstroke, the inertia of the oil volume in the third land skews the oil mass downward towards the OC rails. On the following upstroke, that oil volume skews upwards toward the second ring.

8) Film thickness under the OC rails is clearly observable. The film thickness of the two OC rails is always greater than that of the top two rings. Also, the film thickness under the lower OC rail is greater than that under the upper OC rail regardless of stroke.

9) Absence of the skirt at the window #4 location (midstroke, along wrist pin axis) seems to effect the oil film thickness to viscosity trend. The minimum oil film thickness at the window #4 location does not vary much at all with large changes in viscosity.

## **CHAPTER 10 RECOMMENDATIONS**

### **10.1 FUTURE EXPERIMENTAL WORK**

The following are the author's recommendations of additional experiments that will enhance the current work:

- 1) To study the sensitivity of the ring pack film thicknesses to ring profiles:
  - a) install rings of different face profiles,
  - b) install second ring and OC rails upside-down,
  - c) install second ring with and without the chamfer to study intentional ring twist effects.
- 2) Conduct survey of crown land and second land wet/dryness for a matrix of running conditions, liner temperatures, liner locations, and oil grades.
- 3) Carefully study wear marks on all ring surfaces to deduce dominant tilt conditions.
- 4) OC rail slop within the piston ring groove was assumed to be negligible due to the apparent very tight fit. However, the possibility of ring tilt or twist does exist during radial ring loading, and axial (relative to engine cylinder) pressure and liner friction loading. This type of data was not available at this time, but is recommended for further investigation.
- 5) Study the effects of piston skirt oil drain holes (Chrysler 2.2 engine) vs. piston side skirt drain grooves (Kohler) on circumferential oil behavior under the rings and on the piston lands.
- 6) Study the oil behavior under the rings and on the piston lands during transient operating conditions such as engine speed ramping or abrupt load changes.

### **10.2 LIF SYSTEM RECOMMENDATIONS**

- 1) Investigate reason for why data acquisition of the 3500 rpm data set failed. A possible reason may be that the shaft encoder can not accurately deliver its pulses at high engine speeds (i.e. inadequate frequency response).
- 2) Move top center LIF window down about 5 mm or so to avoid the sludge ring that builds up on the liner, or
- 3) Built an LIF window that spans a few inches along the axis of the liner.

- 4) Use Loctite (low-strength) on focusing probe to prevent vibration loosening during engine operation.
- 5) Re-engineer laser focusing assembly so that the laser can be focused into a thinner beam for better resolution. (Section 6.4.2)
- 6) Along with the new lenses described in (5) above, increase the wall thickness of the probe housing for greater durability and ease of manufacture.

## REFERENCES

- [1] Coy R.C., Michopoulos, Y., Wilkinson, J.P.T., "Environmental Impact of Lubricants", Shell Research Thornton, Published in proceedings of the 21st Leeds/Lyon Symposium of Tribology "Lubricants and Lubrication," Leeds, 1994.
- [2] Coy, R.C., Kirsch, L.J., Bates, T.W., Burnett, P.J., "Automotive Lubrication Studies," Shell Research Thornton, Presented at Austrib '94, December 1994.
- [3] Deutsch, Eric, "Piston Ring Friction Analysis from Oil Film Thickness Measurements," MIT Master's Thesis, Dept. of Mechanical Engineering, February, 1994.
- [4] Shaw, B.T., "Direct Observation of the Oil Consumption Mechanism of a Production Single-Cylinder Diesel Engine," MIT Master's Thesis, Dept. of Mechanical Engineering, February 1992.
- [5] Hout, D.P., Lux, J.P., Wong, V.W., Billian, S.A., "Calibration of Laser Fluorescence Measurements of Lubricant Film Thickness in Engines," SAE paper 881587, 1988.
- [6] Bronchtein, Leon, "Diagnostic Enhancements for the Laser-Induced Fluorescence System," Consortium of Lubrication in Internal Combustion Engines at MIT, October 1993.
- [7] Stubbington, N., "The Photomultiplier as a Versatile Light Detector," SPIE-The International Society for Optical Engineering, 1981.
- [8] Oppenheim, A.V., Schaffer, R.W., "Discrete-Time Signal Processing," Prentice Hall, Inc, 1989.
- [9] Furuhashi, S., Enomoto, Y., "Piston Temperature of Automobile Gasoline Engine in Driving on the Road," Musashi Institute of Technology, 1973.
- [10] French, C.C.J., Atkins, K.A., "Thermal Loading of a Petrol Engine," Presented at the Ordinary Meeting of the Automobile Division, London, 1973.
- [11] Verbal correspondence with Shell technical staff.
- [12] Taylor, R.I., Brown, M.A., Thompson, D.M., Bell, J.C., "The Influence of Lubricant Rheology on Friction in the Piston Ring-Pack," SAE paper # 941981, 1994.
- [13] Bosch Handbook 3rd Edition, 1993, p223
- [14] Tian, T., "Development and Application of Piston Ring-Pack Lubrication Model," Consortium on Lubrication in Internal Combustion Engines at MIT, October 1994.

- [15] Verbal correspondence with Kohler technical staff.
- [16] Brown, M.A., McCann, H., Thompson, D.M., "Characterization of the Oil Film Behavior Between the Liner and Piston of a Heavy-Duty Diesel Engine," SAE paper # 932784, 1993.
- [17] Ryan, J.P., Wong, V.W., Lyon, R. H., Hoult, D.P., Sekiya, Y., Kobayashi, Y., Aoyama, S. "Engine Experiments on the Effects of Design and Operational Parameters on Piston Secondary Motion and Piston Slap," SAE paper 940695, 1994.
- [18] Cameron, A.; *Basic Lubrication Theory*; Ellis Horwood Limited; Chichester, England, 1976.
- [19] Azzola, J.H., "The Role of Surface Tension in the Reduction of Piston Ring Drag," Ph.D Thesis, Department of Mechanical Engineering, MIT 1992.
- [20] Verbal correspondence with Tian Tian at MIT.
- [21] Batchelor, G.K., F.R.S. *An Introduction to Fluid Dynamics*, Cambridge University Press, 1967, p 224.
- [22] Lusted, R.Mark, "Direct Observation of Oil Consumption Mechanisms in a Production Spark Ignition Engine Using Fluorescence Techniques," MIT Master's Degree Thesis, May 1994.
- [23] Private conversation with Tian Tian at MIT.

**Appendix A**  
**COMMON REFERENCE NUMBERS**

- 1) 1 micron = .04 thousandth of inch.
- 2) 25 micron = 1 thousandth of inch.
- 3) LIF dye mixture ratio = for every 2 liters of oil, 0.15 g for Coumarin 523 dye dissolved in 75 ml of dichloromethane.

For baseline running condition of fired-2500rpm, bmep = 631 kPa, 20 Nm load, 100 deg. C at midstroke, thrust side window:

- 4) Typical free-liner oil film thickness in Kohler = 0.3 to 0.5 microns
- 5) Typical top ring minimum oil film thickness in Kohler = 1.0 to 1.8 microns.
- 6) Typical second ring minimum oil film thickness in Kohler = 1.0 to 1.8 microns.
- 7) Typical Upper Oil Control rail minimum oil film thickness in Kohler = 2.0 to 3.2 microns.
- 8) Typical Lower Oil Control rail minimum oil film thickness in Kohler = 2.7 to 5.0 microns.
  
- 9) Typical Oil Consumption for range of I.C. engines = .3 to .5 g/hr per cylinder.

## Appendix B SAMPLE TEST RECORDING SHEET

<b>DATA SET:</b>						
date:	time:	filename:				
OIL						
RPM						
LOAD						
samples:	CLK:EXT	Chn's:0&1	Range =			
#of cycles:	Trig.On: Dig. Edge		Start:after	Edge:Pos.	Trig. At: 0 v	
oil level check:			cal-int	cal-comp	cal-expan	cal-exh
PMT voltage:		x				
laser power:		y				
laser P from fiber:		mv/um				
liner temp (TDC/BDC):						
sump temp:						
zero offset:						
comments:						
		Intake Down	Comp. Up	Pow. Down	Exh. Up.	
	top x					
	top y					
	2nd x					
	2nd y					
	OC x					
	OC-u y					
	OC-l y					
	hinf					
	top ho					
	top h1					
	top h2					
	2nd ho					
	2nd h1					
	2nd h2					
	OC-u ho					
	OC-u h1					
	OC-u h2					
	OC-l ho					
	OC-l h1					
	OC-l h2					

Table B.1 Sample test recording sheet.

**Appendix C**  
**LIF CALIBRATION COEFFICIENTS**  
**[mv/micron]**

	fire-2500 rpm, 100C	fire-2500 rpm, 80C	fire-2500 rpm, 60C	fire-1800 rpm, 100C
win 1, SAE 10W	50	75	75	50
win 1, 10W50	75	75	67	75
win 1, SAE 50	75	75	60	75
win 2, SAE 10W	68			
win 2, 10W50	100			
win 2, SAE 50	100			
win 4, SAE 10W	50			
win 4, 10W50	78			
win 4, SAE 50	80			
win 6, SAE 10W	50			
win 6, 10W50	80			
win 6, SAE 50	75			

**Table C.1** LIF calibration coefficients for fired data sets. The calibration coefficient for each data set was determined from single traces, and was used for all the strokes and cycles. The corresponding PMT voltages are discussed in Section 6.4.4.

## Appendix D ADDITIONAL LIF FILM THICKNESS PLOTS

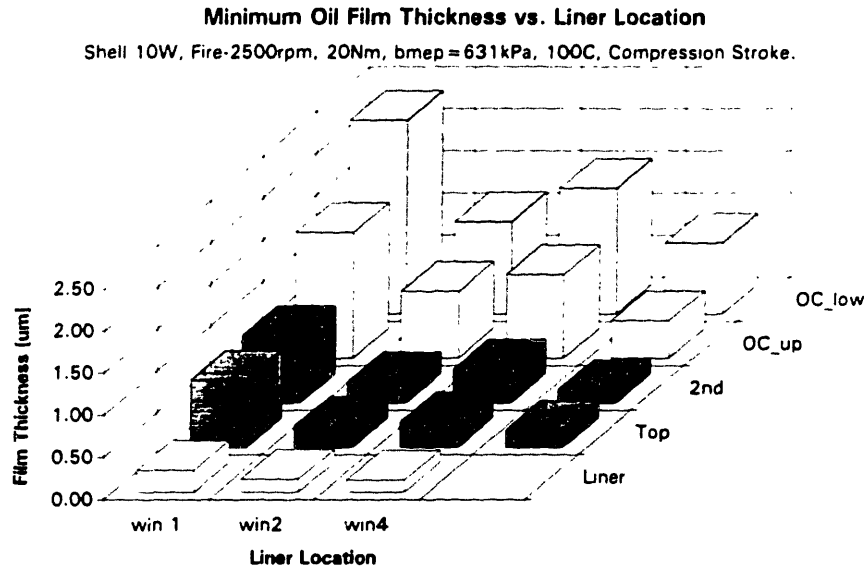


**Figure D.1** MOFT vs. liner location for the compression stroke. Shows trends of: windows (circumferential, axial), rings, speed (mid vs. BDC) for SAE 10w oil. Data has been averaged over ten cycles.

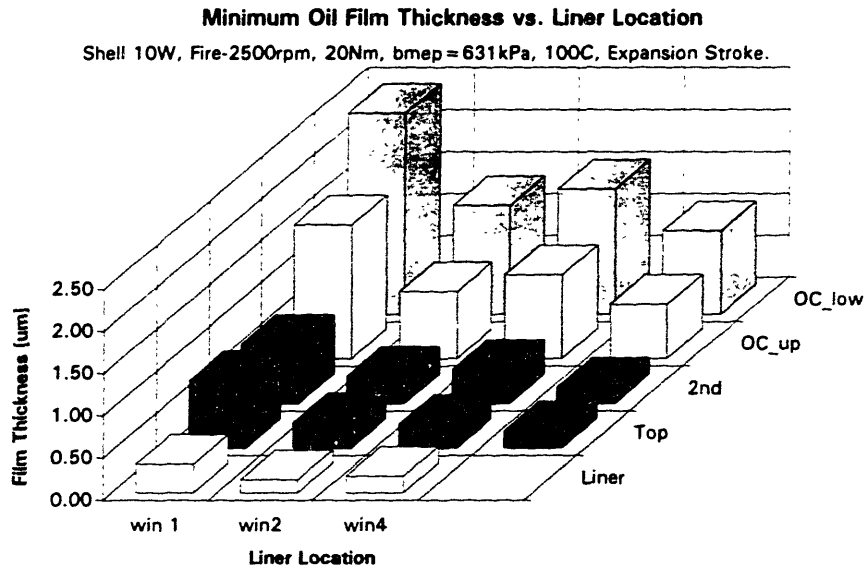


**Figure D.2** MOFT vs. liner location for the expansion stroke. Shows trends of: windows (circumferential, axial), rings, speed (mid vs. BDC) for SAE 10w oil. Data has been averaged over ten cycles.

**Minimum Oil Film Thickness vs. Liner Location**  
 Shell 10W, Fire-2500rpm, 20Nm, bmep = 631kPa, 100C, Exhaust Stroke.

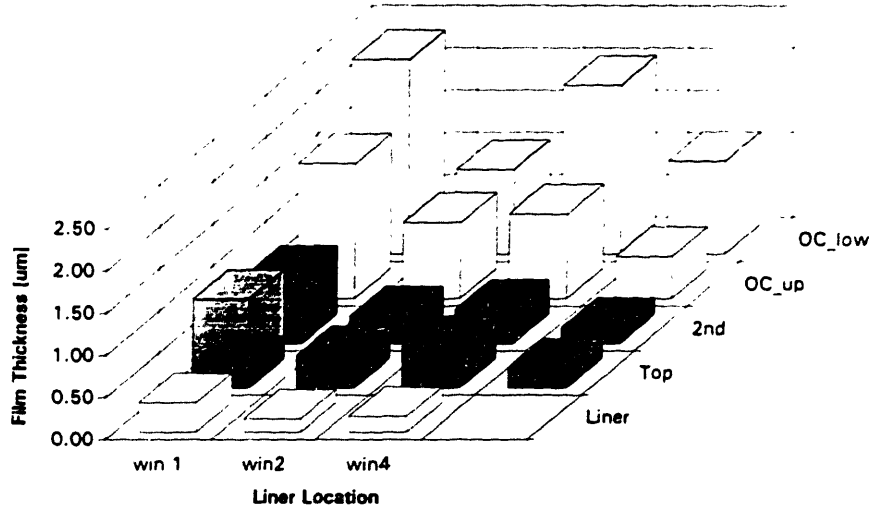


**Figure D.3** MOFT vs. liner location for the exhaust stroke. Shows trends of: windows (circumferential, axial), rings, speed (mid vs. BDC) for SAE 10w oil. Data has been averaged over ten cycles.

**Free-Liner Film Thickness ( $h_{inf}$ ) vs. Oil Grade vs. Liner Location. (Intake Stroke)**

Kohler, Fire-2500rpm, bmep = 631 kPa, 100C.

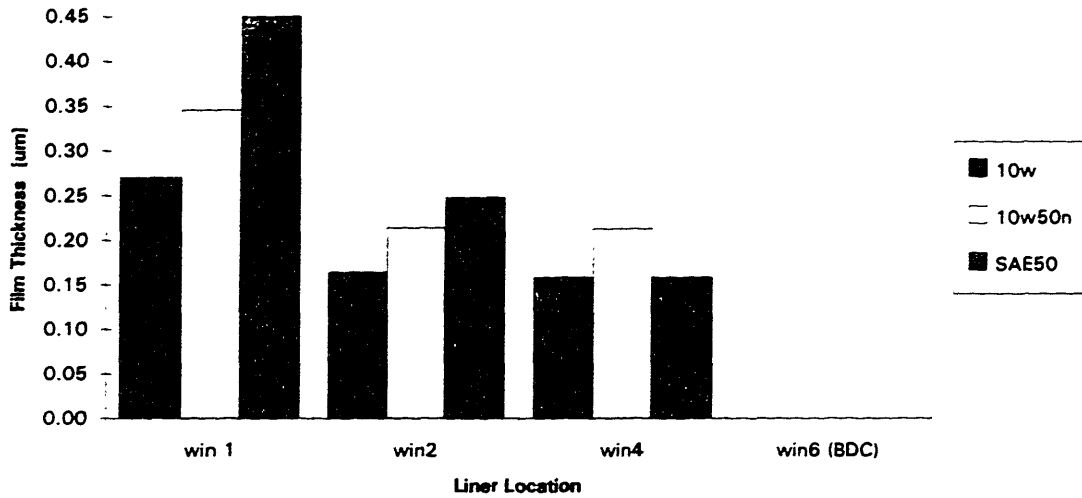


**Figure D.4** Free-liner film thickness vs. oil grade vs. liner location. Shows trend of: windows, skirt, and oil viscosity. Clearly illustrates viscosity trend for each window. Data has been averaged over ten cycles. Recall that the free-liner is not seen from window #6 (BDC).

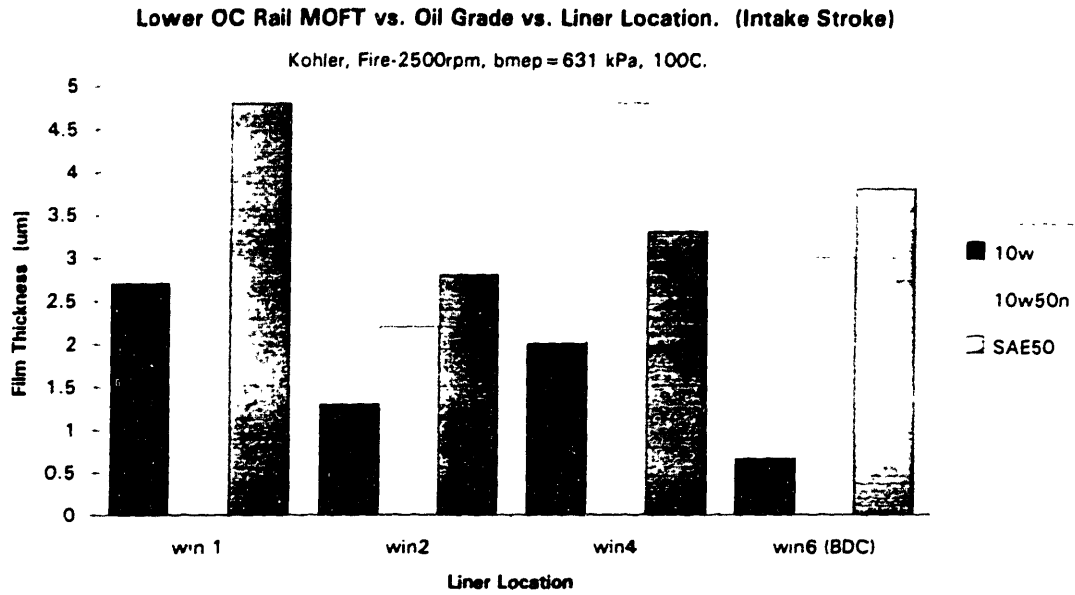


**Figure D.5** Lower OC rail MOFT vs. oil grade vs. liner location. Shows trend of: windows, skirt, and oil viscosity. Clearly illustrates viscosity trend for each window. Data has been averaged over ten cycles.



# THESIS PROCESSING SLIP

FIXED FIELD: ill \_\_\_\_\_ name \_\_\_\_\_

index \_\_\_\_\_ biblio \_\_\_\_\_

► COPIES Archives Aero Dewey Eng Hum  
Lindgren Music Rotch Science

TITLE VARIES ►  \_\_\_\_\_

NAME VARIES ►  \_\_\_\_\_

IMPRINT (COPYRIGHT) \_\_\_\_\_

► COLLATION: 91p

► ADD. DEGREE: \_\_\_\_\_ ► DEPT.: \_\_\_\_\_

SUPERVISORS: \_\_\_\_\_

NOTES:

cat'r: \_\_\_\_\_ date: \_\_\_\_\_

► DEPT: M.E.

page: ► <u>533</u>
-----------------------

► YEAR: 1995 ► DEGREE: M.S.

► NAME: TAMAI, Goro